

# scE<sup>2</sup>TM: Toward Interpretable Single-Cell Embedding via Topic Modeling

Hegang Chen<sup>1</sup>, Yuyin Lu<sup>1</sup>, Zhiming Dai<sup>1</sup>, Fu Lee Wang<sup>2</sup>,  
Qing Li<sup>3</sup>, Yanghui Rao<sup>1\*</sup>

<sup>1\*</sup>School of Computer Science and Engineering, Sun Yat-sen University,  
132 Waihuan East Road, Guangzhou, 510006, China.

<sup>2</sup>School of Science and Technology, Hong Kong Metropolitan  
University, Mong Man Wai Building, Hong Kong, 999077, China.

<sup>3</sup>Department of Computing, The Hong Kong Polytechnic University,  
Street, Hong Kong, 610101, China.

\*Corresponding author(s). E-mail(s): [raoyangh@mail.sysu.edu.cn](mailto:raoyangh@mail.sysu.edu.cn);  
Contributing authors: [chenhg25@mail2.sysu.edu.cn](mailto:chenhg25@mail2.sysu.edu.cn);  
[luyy37@mail2.sysu.edu.cn](mailto:luyy37@mail2.sysu.edu.cn); [daizhim@mail.sysu.edu.cn](mailto:daizhim@mail.sysu.edu.cn);  
[pwang@hkmu.edu.hk](mailto:pwang@hkmu.edu.hk); [csqli@comp.polyu.edu.hk](mailto:csqli@comp.polyu.edu.hk);

## Abstract

Recent advances in sequencing technologies have enabled researchers to explore cellular heterogeneity at single-cell resolution. Meanwhile, interpretability has gained prominence parallel to the rapid increase in the complexity and performance of deep learning models. In recent years, topic models have been widely used for interpretable single-cell embedding learning and clustering analysis, which we refer to as single-cell embedded topic models. However, previous studies evaluated the interpretability of the models mainly through qualitative analysis, and these single-cell embedded topic models suffer from the potential problem of interpretation collapse. Furthermore, their neglect of external biological knowledge constrains analytical performance. Here, we present scE<sup>2</sup>TM, an external knowledge-guided single-cell embedded topic model that provides a high-quality cell embedding and strong interpretation, contributing to comprehensive scRNA-seq data analysis. Our comprehensive evaluation across 20 scRNA-seq datasets demonstrates that scE<sup>2</sup>TM achieves significant clustering performance gains compared to 7 state-of-the-art methods. In addition, we propose a new interpretability evaluation benchmark that introduces 10 metrics to quantitatively assess the interpretability of single-cell embedded topic models. The results show that the interpretation provided by scE<sup>2</sup>TM performs encouragingly in terms of

diversity and consistency with the underlying biological signals, contributing to a better revealing of the underlying biological mechanisms.

**Keywords:** Single-cell embedded topic model, External knowledge, Interpretation collapse, Interpretability evaluation

## 1 Introduction

Advances in single-cell sequencing technologies have revolutionized our ability to interrogate biological systems at unprecedented resolution [1, 2]. As an important application of single-cell RNA sequencing (scRNA-seq) data, unsupervised clustering has emerged as a powerful tool for de novo cell-type identification, revealing previously uncharacterized cellular states [3]. Deep learning has garnered significant attention in the single-cell community for its remarkable ability to process sparse, noisy, and high-dimensional single-cell data [4]. Despite its success, the inherent complexity of multi-layer nonlinear architectures, activation functions, and large parameter spaces often renders deep learning-based models black boxes [5]. This lack of model interpretability poses a significant challenge to establishing public trust and verifying accuracy in the fields of molecular biology and biomedicine.

In response to this challenge, interpretable deep learning has gained prominence in biological data analytics, where the core goal is to develop models capable of generating, interpreting, and presenting their decision-making processes or data insights in a human-understandable manner [6–9]. In recent years, topic modeling has been successfully applied in the field of bioinformatics [10–12], encompassing applications such as single-cell data analysis and electronic health record processing. Originally developed for mining textual data [13–16], the appeal of topic modeling lies in its ability to efficiently handle high-dimensional sparse data while providing interpretability by associating input features with latent factors or target outcomes through discovered topics. Within single-cell analysis, a series of studies have integrated deep learning-based embedding techniques with topic modeling, leading to the development of various single-cell embedded topic models [10, 17–22]. For instance, scETM [10] pioneered the adaptation of topic modeling, utilizing interpretable linear decoders to learn highly interpretable gene and topic embeddings. Building upon this, d-scIGM [20] enhances the model’s capacity to capture latent data signals by employing deeper neural network architectures, thereby better modeling the dependencies between topics and genes. Other notable applications include MIRA [17], which combines topic modeling of cell states with regulatory potential modeling of gene loci, and STAMP [23], which constructs an interpretable spatial perceptual downscaling method based on the prodLDA topic model [24] to identify biologically relevant low-dimensional spatial topics and associated gene modules. While the integration of the topic modeling with the single-cell domain has made promising progress in the interpretable embedding and clustering analysis of single-cell data, several challenges remain for existing single-cell embedded topic models.

**The first challenge is the lack of explicit metrics to quantify the interpretability of single-cell embedded topic models.** While single-cell embedded topic modeling improves the interpretability of the cell embedding process through the introduction of topics, a fundamental tension arises between the objectives of topic modeling and single-cell clustering. Specifically, topic modeling prioritizes the discovery of well-defined, interpretable topics, whereas single-cell clustering methods primarily focus on learning discriminative cell representations that facilitate cell type separation [25, 26]. Furthermore, current evaluations of single-cell embedded topic models rely predominantly on qualitative analyses of the model-derived interpretations, making it challenging to systematically assess whether the optimization process for cellular representations compromises interpretation quality. The latest reviews [27, 28] further highlight the potential for bias and incomplete understanding inherent in solely qualitative approaches to interpretability assessment. Consequently, developing quantitative metrics for evaluating the interpretability of these models remains a significant and under-explored challenge.

**The second challenge is the potential interpretation collapse problem in existing single-cell embedded topic models.** These models, inspired by topic discovery in natural language processing (NLP), derive their interpretability from the identified topics. However, recent NLP research [29] highlights that words in document collections typically follow a long-tailed distribution, characterized by a small number of high-frequency words and a large number of low-frequency words. Since topic and word embeddings are learned by minimizing the reconstruction loss, this skewed distribution can cause the optimization process to disproportionately emphasize high-frequency words. Consequently, most learned topic embeddings tend to converge semantically towards the embeddings of these high-frequency words, resulting in topics exhibiting low semantic diversity, a phenomenon known as interpretation collapse. Notably, scRNA-seq data exhibits a similar long-tailed distribution in gene expression [30]. This parallel suggests that single-cell embedded topic models are susceptible to the same interpretation collapse problem, manifesting in two key ways: (i) models disproportionately emphasize highly expressed genes, leading to redundant identification of common gene programs while failing to capture diverse interpretations; and (ii) these models struggle to fully explore the potential biological signals in single-cell data, and the interpretations found cannot accurately reflect the real cell properties.

**The third challenge lies in moving beyond current paradigms to better guide embedding learning.** Although deep embedding methods such as scDHA [31] and d-scIGM [20] effectively model high-dimensional, sparse scRNA-seq data, they primarily focus on cellular expression profiles, often overlooking intercellular structural information. To incorporate relational information directly into the latent representation, several methods have employed Graph Neural Networks (GNNs) as encoders. These GNNs integrate neighboring cell information within the latent space, providing additional supervision for model optimization. For example, scTAG [32] constructs a cell-cell network from expression data and utilizes a topology-adaptive graph-convolutional autoencoder with a zero-inflated negative binomial model to learn low-dimensional embeddings, which are then spectrally clustered to refine the model. Similarly, scLEGA [33] integrates two distinct scRNA-seq clustering strategies using

multi-head attention. However, a key limitation of these graph-based methods is their reliance solely on internal gene expression data to construct cellular networks, constraining them by the inherent informational limitations of the input data. Importantly, the recent emergence of single-cell foundation models [34, 35] highlights the availability of abundant external knowledge that could assist in analysis. This rich, diverse external knowledge offers a promising source of supervisory signals for more effectively guiding embedding and clustering.

In this paper, we propose 10 quantitative metrics to evaluate the interpretability of single-cell embedded topic models from diverse perspectives, which together with the clustering metrics form a more systematic evaluation framework. Our comprehensive assessment reveals that existing single-cell embedded topic models suffer from interpretation collapse, a phenomenon where topics fail to capture distinct biological patterns. Furthermore, by systematically analyzing the metrics of clustering and interpretability, we discover that these metrics are barely correlated, which suggests that previous single-cell embedded topic models do not guarantee the quality of interpretation while pursuing a high clustering performance, further demonstrating the importance of the quantitative evaluation of interpretability. Based on these insights, we present **scE<sup>2</sup>TM** (**E**xternal knowledge-guided **E**mbedding clustering regularization **T**opic **M**odel for **s**ingle-cell analysis), a deep generative model for large-scale single-cell transcriptomic analysis, as shown in Fig. 1. To alleviate interpretation collapse, we introduce **E**mbedding **C**lustering **R**egularization (**ECR**), a module that regularizes topic embeddings into clustering centers and gene embeddings into clustering samples, and models cluster soft assignments via an Optimal Transport (OT) formulation. This forces topics to diverge rather than collapse, enhancing their capacity to represent distinct biological processes. The emergence of foundation models is transforming deep learning: instead of adopting the internal guidance paradigm that uses cell networks to introduce structural information to supervise model optimization, our scE<sup>2</sup>TM integrates the rich external knowledge brought by single-cell foundation models through a cross-view mutual distillation strategy, which is an external guidance paradigm with enhanced performance and scalability. Evaluated across 20 datasets spanning diverse tissues and sizes, scE<sup>2</sup>TM exhibits state-of-the-art performance in both clustering accuracy and interpretability.

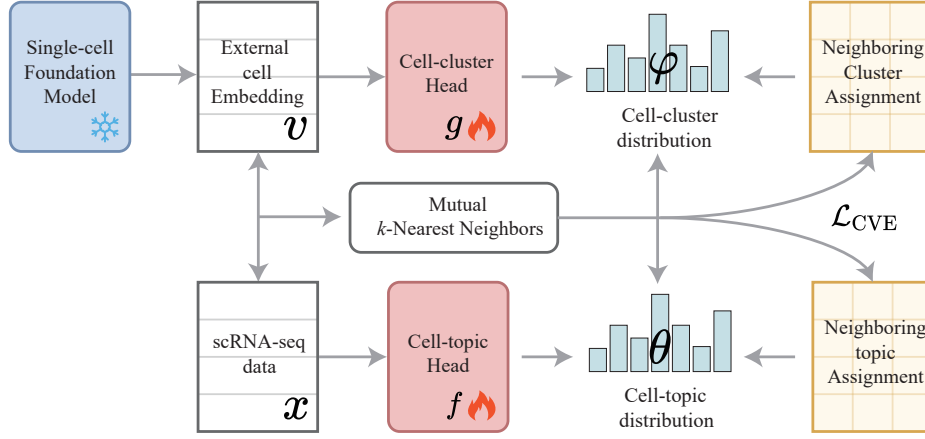
## 2 Results

### 2.1 Overview of Interpretability Evaluation Benchmarks and scE<sup>2</sup>TM

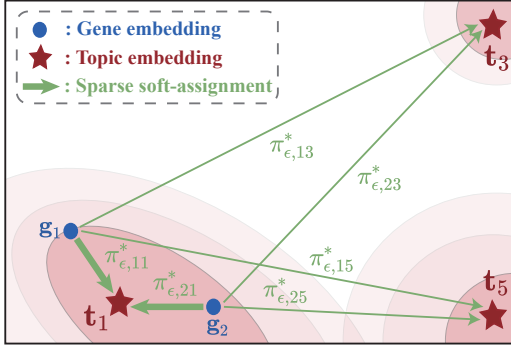
We propose new interpretability assessment benchmarks to quantify the interpretability of single-cell embedded topic models and develop scE<sup>2</sup>TM to model scRNA-seq data. Our approach addresses 3 key challenges:

- **RQ1:** How to evaluate the interpretation quality of single-cell embedded topic models?
- **RQ2:** How to mitigate the critical problem of interpretation collapse?

(a) Cross-view Encoder



(b) Embedding Clustering Regularization



(c) Sparse Linear Decoder

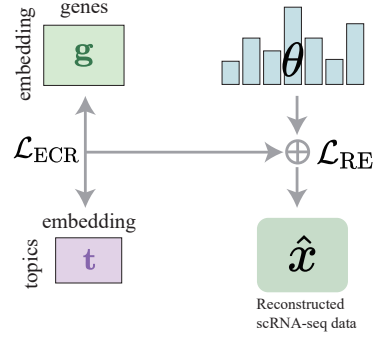


**Fig. 1** Schematic overview of scE<sup>2</sup>TM. (a) To better collaborate the information of different perspectives, clusters and topic heads are trained based on the mutual neighborhood information by encouraging consistent clustering assignments of mutual nearest neighbors of the corresponding cells of different perspectives in the embedding space. (b) ECR clusters gene embeddings  $\mathbf{g}_j$  (•) as samples and topic embeddings  $\mathbf{t}_k$  (★) as centers with soft-assignment  $\pi_{\epsilon,jk}^*$ . Here ECR pushes  $\mathbf{g}_1$  and  $\mathbf{g}_2$  close to  $\mathbf{t}_1$  and away from  $\mathbf{t}_3$  and  $\mathbf{t}_5$ . (c) Sparse linear decoders learn topic embeddings and gene embeddings as well as sparse topic-gene dependencies during reconstruction, thus ensuring model interpretability.

- **RQ3:** How to utilize external knowledge for enhancing the performance of cell clustering?

In previous analyses of single-cell data, biologists have tended to validate partial interpretations captured by interpretable models through qualitative analyses, focusing primarily on whether models generate diverse interpretations and whether those interpretations reflect the underlying biological properties of the data [36, 37]. To extend this qualitative approach with rigorous quantification, we introduce 10 quantitative metrics designed to comprehensively evaluate the interpretability of

model-derived topics. These metrics assess interpretability from multiple perspectives, including the consistency between identified cellular topics and cell types, coherence and diversity of the topics, and the capability of topics to capture biological pathways.

Building upon the foundation of our quantitative interpretability benchmarks, we further propose scE<sup>2</sup>TM, an innovative single-cell embedded topic model designed to address key challenges in interpretability and performance. To alleviate the interpretation collapse problem, we introduce the ECR module, adapted from the topic model ECRTM [29]. Particularly, ECR (Fig. 1b) simulates soft cluster assignments through the solution of a tailored OT problem defined between the topic embeddings and gene embeddings. This mechanism forces each topic embedding to become the center of a distinct cluster of aggregated gene embeddings, ensuring the topics are well-separated and encompass diverse semantic spaces, thereby directly combating interpretation collapse. Within ECR,  $K$  topic embeddings serve as cluster centroids and  $V$  gene embeddings represent the data points. Let  $n_k$  denote the number of genes assigned to topic embedding  $\mathbf{t}_k$ , and  $s_k = n_k/V$  represent the corresponding cluster size proportion. The vector  $\mathbf{s} = (s_1, \dots, s_K)^\top \in \Delta_K$  summarizes all cluster size proportions. Notably, there is usually a lack of a priori knowledge about the cluster sizes of topics. However, previous research [29, 38] finds that setting all cluster sizes to unity:  $n_k = V/K$ ,  $\mathbf{s} = (1/K, \dots, 1/K)^\top$  can avoid trivial solutions with empty clusters.

To extract the knowledge of cells and their associations embedded in the single-cell foundation model, we first consider the scRNA-seq transcriptome data  $\mathbf{x}$  and the external cell embeddings  $\mathbf{v}$  derived from foundation models as cell representations from different perspectives. The corresponding cells and their neighbors from different perspectives are then assigned to the same topic/cluster through a cross-view mutual distillation strategy (Fig. 1a), thus leveraging external knowledge to better guide embedding learning. Compared to previous GNN-based approaches [32, 33], scE<sup>2</sup>TM offers greater flexibility and scalability, and better overall performance.

## 2.2 Quantitative Assessment of Interpretability

### 2.2.1 Topic Coherence

Topic Coherence (TC) quantifies the semantic consistency of a topic by measuring the statistical co-occurrence patterns of its characteristic terms. For a given topic, TC evaluates whether its top-associated terms frequently co-appear in relevant contexts within an external corpus, indicating a coherent semantic representation. This metric strongly correlates with human interpretability judgments in traditional topic modeling [39]. We adapt TC to single-cell biology by leveraging biological pathways as semantic units, using the GASE database [40] as the external knowledge base. Specifically, we suggest that genes assigned to the same topic collaboratively participate in common biological pathways. Formally, TC is defined as

$$\text{TC} = \frac{1}{K} \sum_{k=1}^K \frac{2}{h(h-1)} \sum_{i=1}^h \sum_{j=i+1}^h F(\mathbf{g}_i^{(k)}, \mathbf{g}_j^{(k)}), \quad (1)$$

where  $\{\mathbf{g}_1^{(k)}, \dots, \mathbf{g}_h^{(k)}\}$  denotes the top- $h$  most likely genes in the  $k$ -th topic. And the correlation of word pairs is estimated as follows:

$$F(\mathbf{g}_i, \mathbf{g}_j) = \frac{\log \frac{P(\mathbf{g}_i, \mathbf{g}_j)}{P(\mathbf{g}_i)P(\mathbf{g}_j)}}{-\log(P(\mathbf{g}_i, \mathbf{g}_j))}, \quad (2)$$

where  $P(\mathbf{g}_i, \mathbf{g}_j)$  is the probability that genes  $\mathbf{g}_i$  and  $\mathbf{g}_j$  co-occur in the same biological process, and  $P(\mathbf{g}_i)$  is the marginal probability of gene  $\mathbf{g}_i$ . TC ranges continuously on  $[0, 1]$ , with higher values indicating superior coherence.

### 2.2.2 Topic Diversity

Topic Diversity (TD) quantifies the distinctness of biological mechanisms captured by different topics. While existing single-cell embedded topic models often suffer from interpretation collapse, i.e., the model mines many overlapping topics. Therefore, topic diversity should be one of the important metrics for assessing interpretability. Formally, TD is defined as follows:

$$\text{TD} = \frac{|\text{Unique}(M)|}{|M|}, \quad (3)$$

where  $M = \bigcup_{k=1}^K \{\mathbf{g}_1^{(k)}, \dots, \mathbf{g}_h^{(k)}\}$  denotes the gene pool containing the top- $h$  genes corresponding to all topics.  $|M|$  and  $|\text{Unique}(M)|$  denote the number of all genes and the number of unique genes, respectively. TD ranges continuously over  $[0, 1]$ , where  $\text{TD} \rightarrow 0$  indicates high redundancy and  $\text{TD} \rightarrow 1$  reflects maximal diversity.

### 2.2.3 Topic Quality

There is a mutual trade-off between topic coherence and topic diversity in the text mining domain [41], and we suggest that this phenomenon also exists in the single-cell domain. Since some important genes correspond to multiple gene programs, these genes may appear in different topics at the same time, which would result in a higher TC score but a slightly reduced TD score. In addition, specific gene programs may be captured repeatedly by topics, which would further exacerbate the above problem. Therefore, we define the product of topic diversity and topic coherence as the overall Topic Quality (TQ) following Dieng et al. [41], i.e.,

$$\text{TQ} = \text{TC} \times \text{TD}, \quad (4)$$

which ranges from 0 to 1, with higher values indicating superior balance between coherent biological pathways and diverse functional coverage.

### 2.2.4 Interpretation Purity

Interpretation Purity (IP) captures the intuition that cells assigned to the same topic should share common biological characteristics. Specifically, it tests the hypothesis

that dominant topic assignments should align with known cell type annotations at a coarse-grained level, reflecting shared functional states. Adapted from the cluster purity metric, IP quantifies this alignment as:

$$\text{IP}(\Omega, \mathbf{Y}) := \frac{1}{n} \sum_{k=1}^K \max_j |\Omega_k \cap \mathbf{Y}_j|, \quad (5)$$

where  $\Omega = \{\Omega_k \mid k = 1, \dots, K\}$  denotes the topic assignments with  $\Omega_k = \{i \mid \arg \max_j \theta_{ij} = k, i = 1, \dots, n\}$  representing cells assigned to topic  $k$ . Besides,  $\mathbf{Y} = \{\mathbf{Y}_j \mid j = 1, \dots, J\}$  represents  $J$  ground truth cell types with  $\mathbf{Y}_j$  containing cells of type  $j$ . And  $n$  is the total number of cells. The metric ranges within  $[0, 1]$ , where higher values indicate stronger agreement between topics and biological cell states, reflecting more meaningful cellular interpretations.

### 2.2.5 Quality of Topic Over-representation Analysis

Complementing the cell-level assessment of interpretation purity, which measures the alignment of topics with biological cell states, we now evaluate the functional relevance of topics at the gene and pathway level. To validate the biological mechanisms captured by mined topics, we perform Over-Representation Analysis (ORA) that statistically evaluates whether top topic-associated genes cluster significantly in known biological pathways. This quantifies how effectively topics capture interpretable biological mechanisms. Specifically, we propose three complementary metrics that assess different dimensions of this functional enrichment quality: (i) number of unique pathways enriched by topic ( $\text{ORA}_N$ ) measures the breadth of distinct biological functions captured across all topics; (ii) uniqueness of topic enrichment pathway ( $\text{ORA}_U$ ) quantifies avoidance of pathway repetition; and (iii) the quality of topic over-representation analysis ( $\text{ORA}_Q$ ) balances the assessment in both coverage and uniqueness. The formal definitions of these metrics are as follows:

$$\text{ORA}_N = |\text{Unique}(P_O)|, \text{ORA}_U = \frac{|\text{Unique}(P_O)|}{|P_O|}, \text{ORA}_Q = \text{ORA}_N \times \text{ORA}_U, \quad (6)$$

where  $P_O$  contains the topic enrichment pathways obtained via ORA.  $|P_O|$  and  $|\text{Unique}(P_O)|$  denote the number of all pathways and the number of unique pathways, respectively. Similar to TQ,  $\text{ORA}_Q$  is defined as the product of  $\text{ORA}_N$  and  $\text{ORA}_U$ .

### 2.2.6 Quality of Topic Gene Set Enrichment Analysis

While ORA evaluates pathway enrichment using thresholded top genes, this approach requires arbitrary selection of gene cutoffs [10, 20]. To overcome this limitation, we conduct Gene Set Enrichment Analysis (GSEA), a threshold-free method that evaluates enrichment across the entire ranked list of genes sorted by their association strength with each topic. GSEA computes a running enrichment score that avoids discrete gene selection, providing more robust pathway associations (method details in Supplementary Note 1). Following our ORA evaluation framework, we adapt three

analogous metrics ( $GSEA_N$ ,  $GSEA_U$ ,  $GSEA_Q$ ) to quantify biological interpretability:

$$GSEA_N = |\text{Unique}(P_G)|, GSEA_U = \frac{|\text{Unique}(P_G)|}{|P_G|}, GSEA_Q = GSEA_N \times GSEA_U, \quad (7)$$

where  $P_G$  contains the topic enrichment pathways obtained via GSEA.

### 2.3 Interpretability Evaluation Benchmarks Quantify the Potential Risk of Interpretational Collapse.

In this section, we use the proposed interpretability evaluation benchmarks (i.e., IP, TC, TD, TQ,  $ORA_N$ ,  $ORA_U$ ,  $ORA_Q$ ,  $GSEA_N$ ,  $GSEA_U$ , and  $GSEA_Q$ ) to quantify the interpretability of single-cell embedded topic models. As shown in Fig. 2 and Supplementary Fig. 1, scE<sup>2</sup>TM achieves the best interpretable performance overall, substantially outperforming the second best method in terms of IP (8.6% performance gain), TQ (66.5% performance gain),  $GSEA_Q$  (27.5% performance gain) and  $ORA_Q$  (16.1% performance gain).

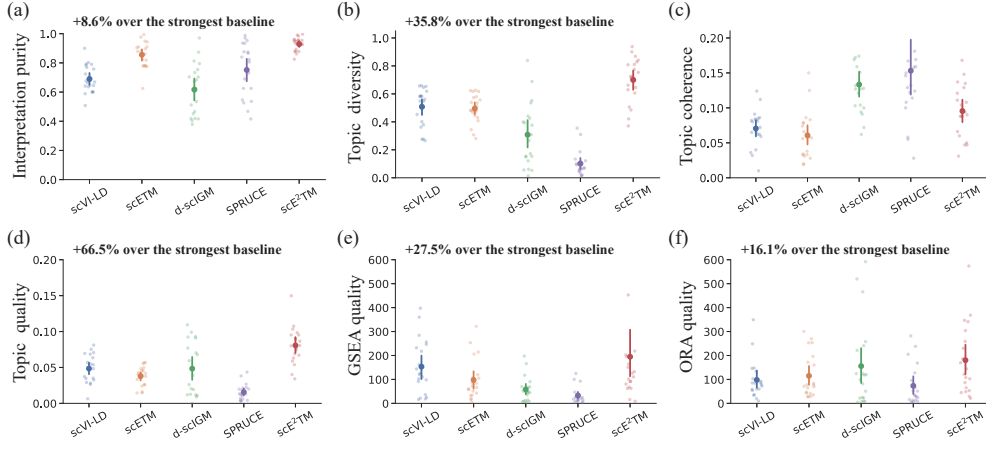


**Fig. 2** Quantitative evaluation of interpretability for single-cell embedded topic models using six core metrics: (a) Interpretation purity, (b) Topic diversity, (c) Topic coherence, (d) Topic quality, (e) GSEA quality, and (f) ORA quality.

We observe very low IP values for scVI-LD and d-scIGM (Fig. 2a), even compared to the SPRUCE model with the lowest TQ (Fig. 2d), suggesting that the interpretations mined by these models do not reflect the cell type information well, and that they may not accurately capture real biological signals. Furthermore, the topic diversity of d-scIGM and SPRUCE is poor (Fig. 2b), even close to 0.1 in some datasets, while their overall TC scores (Fig. 2c) are very high, indicating that these methods repeatedly mined a few specific high TC gene programs and are not able to comprehensively explore single-cell data. This is further supported by the quantitative results of GSEA

and ORA, which show that d-scIGM and SPRUCE, although enriched for a larger number of pathways (Supplementary Fig. 1a and b), have a very high repetition rate of these pathways (Supplementary Fig. 1c and d). In summary, previous single-cell embedded topic models do suffer from interpretation collapse, and scE<sup>2</sup>TM effectively mitigates the problem and significantly improves the quality of interpretation.

## 2.4 scE<sup>2</sup>TM Provides High-quality Cell Embedding.

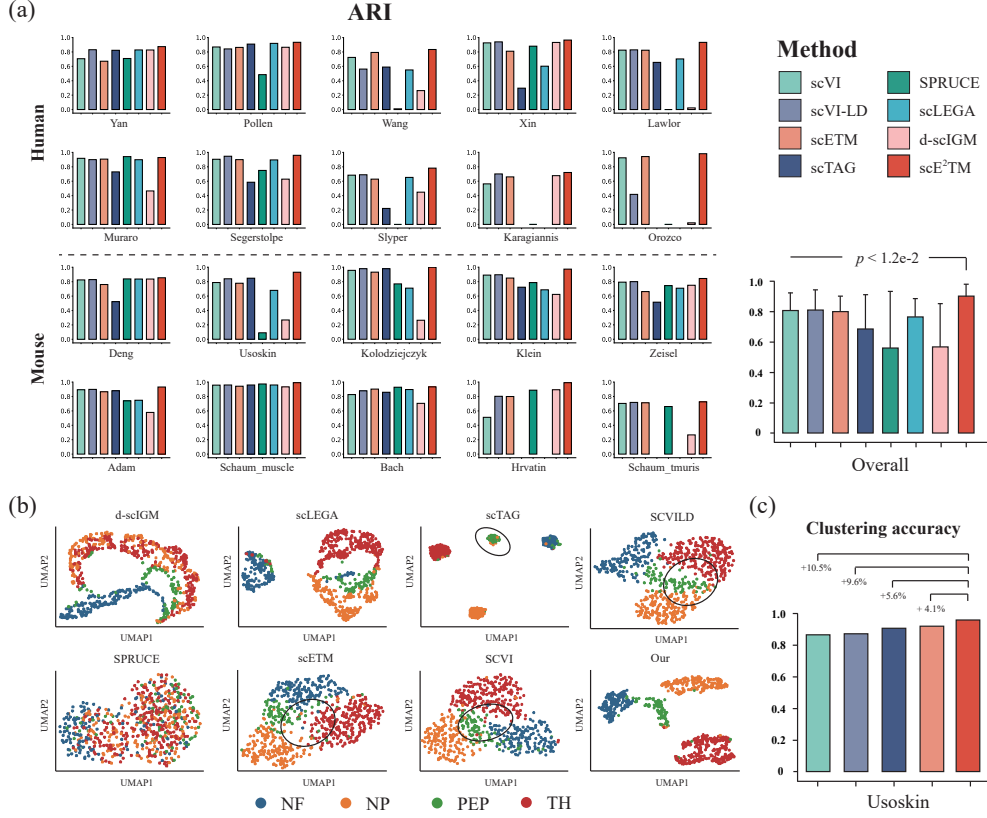
We benchmark scE<sup>2</sup>TM against 7 state-of-the-art single-cell analysis methods on 20 scRNA-seq datasets. Comparative results show that scE<sup>2</sup>TM significantly outperforms all baselines, with ARI 11.3% ( $p$ -value =  $1.2\text{e-}2$ ) higher and NMI 8.7% ( $p$ -value =  $1.7\text{e-}2$ ) higher than the top-performing benchmark (Fig. 3a and Supplementary Fig. 2). Furthermore, methods like SPRUCE and d-scIGM exhibit high performance variance across datasets (Fig. 3a, error bars), indicating their sensitivity to data characteristics. In contrast, our method is more stable and exhibits consistently superior performance. Interestingly, methods integrating cell network (e.g., scTAG, scLEGA) do not consistently outperform expression-only models, and their computational demands limit scalability to large datasets such as Karagiannis, Orozco. Notably, scE<sup>2</sup>TM surpasses the cell network-integrated method scLEGA by 18.1% in ARI and 14.1% in NMI, attributable to scE<sup>2</sup>TM’s external knowledge-guided embedding paradigm and cross-view encoder design, which more effectively leverages biological prior knowledge compared to scLEGA’s reliance on internally constructed cell networks.

Next, we show the differences between scE<sup>2</sup>TM and the baseline model through visual analysis on the Usoskin dataset, which is selected for its well-defined cell type boundaries. As shown in Fig. 3b, scE<sup>2</sup>TM’s embeddings better capture biological variation under distinct conditions, whereas representative methods like scETM, scVI, and scVI-LD fail to distinguish overlapping populations (highlighted in black circles). To quantify these results, we also assess the per-cell-type clustering accuracy when the predicted cluster number matches the true cell type count. Fig. 3c illustrates that scE<sup>2</sup>TM achieves the highest mean accuracy, further validating its embedding quality.

## 2.5 Correlation Analysis between Metrics Uncovers the Complementarity of Interpretability and Clustering Evaluation.

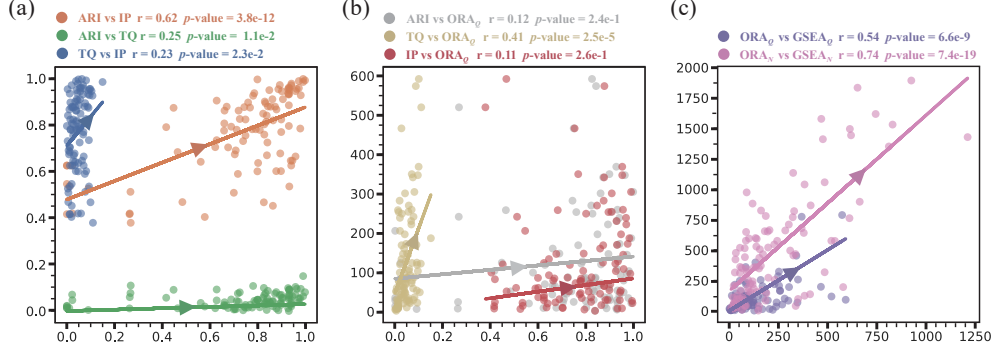
To gain a deeper insight into the metrics and the relationships between different metrics, such as the relationship between the proposed interpretability assessment benchmark and the existing clustering assessment system, as well as the relationship between the interpretability metrics, we analyze correlations between evaluation metrics using Pearson’s correlation coefficient. Specifically, we compute pairwise correlations across all datasets based on each method’s metric scores.

Fig. 4a and Supplementary Fig. 3 demonstrate that IP strongly correlates with clustering metrics (ARI and NMI;  $r > 0.6$ ,  $p < 0.001$ ). It is worth noting that despite the strong correlation between IP and clustering metrics, there is a need to assess interpretation purity. For instance, although scVI-LD has good topic quality and clustering performance, it achieves the second lowest IP. Oppositely, TQ and topic enrichment



**Fig. 3** Clustering and visualization. (a) Evaluating clustering performance with ARI. The 20 panels on the left show the ARI values for the different methods on individual dataset, and the right panel shows the average ARI values and standard deviations, with statistical significance tested by pairwise Whitman U-test. We do not report the results of scTAG and scLEGA on some large scRNA-seq datasets (Karagiannis, Orozco, Hrvatin, and Schaum\_tmuris) because they are out of memory. (b) UMAP visualization of all benchmark models on the Usoskin dataset. (c) Comparison of identifying different cell types, with percentages indicating the degree of accuracy improvement of our scE<sup>2</sup>TM relative to the baseline model.

quality (Fig. 4b and Supplementary Fig. 4) exhibit no significant association with either clustering metric ( $|r| < 0.3$ ). This indicates that high clustering performance does not imply biologically meaningful interpretations, which further illustrates the importance of conducting quantitative interpretability assessments. Furthermore, we observe a correlation between TQ and the quality of the topic enrichment analyses ( $ORA_Q$  and  $GSEA_Q$ ), and Fig. 4c illustrates similar results captured by  $ORA$  and  $GSEA$ , which are consistent with our intuition. Besides, we analyze the relationship between topic coherence and diversity as well as the number of pathways ( $ORA_N$  /  $GSEA_N$ ) and uniqueness of topic enrichment ( $ORA_U$  /  $GSEA_U$ ), and the results (Supplementary Fig. 5) show that there is a significant negative correlation between them, which is in line with previous work [41].



**Fig. 4** Correlation analysis between interpretability and clustering metrics. Pearson correlation coefficients ( $r$ ) quantify association strength, with distinct colors representing different metric pairs.

## 2.6 Different Modules Contribute to scE<sup>2</sup>TM Clustering and Interpretability Performance.

To analyze the contribution of each component in our scE<sup>2</sup>TM, we conduct ablation studies with four cases: (i) Removing the embedding clustering regularization module (w/o ECR). (ii) Deleting the cross-view encoder (w/o CVE). (iii) Replacing the cross-view distillation strategy with the embedded connectivity (w/ EC). (iv) Utilizing external embeddings obtained from the underlying single cells (scGPT). Table 1 summarizes the average metrics for these 4 ablation cases of scE<sup>2</sup>TM.

**Table 1** Comprehensive ablation analysis across all datasets. Performance metrics shown as mean  $\pm$  standard deviation. scGPT produces cell embeddings but not probabilistic topic models, precluding direct comparison on topic interpretability metrics.

Model	ARI	NMI	TC	TD	TQ	IP	ORA <sub>U</sub>	ORA <sub>N</sub>	ORA <sub>Q</sub>	GSEA <sub>U</sub>	GSEA <sub>N</sub>	GSEA <sub>Q</sub>
scGPT	0.681 $\pm$ 0.23	0.712 $\pm$ 0.18	-	-	-	-	-	-	-	-	-	-
scE <sup>2</sup> TM w/o ECR	0.862 $\pm$ 0.10	0.862 $\pm$ 0.07	<b>0.147</b> $\pm$ 0.05	0.597 $\pm$ 0.15	0.068 $\pm$ 0.02	0.916 $\pm$ 0.05	0.612 $\pm$ 0.26	<b>380</b> $\pm$ 308	<b>207</b> $\pm$ 175	<b>0.424</b> $\pm$ 0.25	688 $\pm$ 582	<b>213</b> $\pm$ 219
scE <sup>2</sup> TM w/o CVE	0.843 $\pm$ 0.09	0.845 $\pm$ 0.07	0.119 $\pm$ 0.04	0.700 $\pm$ 0.13	0.080 $\pm$ 0.02	0.913 $\pm$ 0.05	<b>0.694</b> $\pm$ 0.21	304 $\pm$ 253	180 $\pm$ 160	0.354 $\pm$ 0.27	750 $\pm$ 580	179 $\pm$ 156
scE <sup>2</sup> TM w/ EC	0.858 $\pm$ 0.10	0.856 $\pm$ 0.08	0.122 $\pm$ 0.04	<b>0.706</b> $\pm$ 0.14	<b>0.084</b> $\pm$ 0.02	0.929 $\pm$ 0.04	0.683 $\pm$ 0.23	320 $\pm$ 256	198 $\pm$ 165	0.367 $\pm$ 0.27	751 $\pm$ 587	200 $\pm$ 230
scE <sup>2</sup> TM	<b>0.908</b> $\pm$ 0.08	<b>0.888</b> $\pm$ 0.07	0.122 $\pm$ 0.04	0.690 $\pm$ 0.15	0.081 $\pm$ 0.03	<b>0.930</b> $\pm$ 0.04	0.677 $\pm$ 0.21	299 $\pm$ 230	180 $\pm$ 142	0.354 $\pm$ 0.257	<b>758</b> $\pm$ 586	195 $\pm$ 216

ECR ablation (w/o ECR) substantially reduces the diversity of interpretations, demonstrating its critical role in mitigating interpretation collapse. Mechanistically, the ECR module minimizes repetition of key genes across topics by enforcing geometric compactness between topic embeddings and their associated gene embeddings. ORA focuses on the top genes, so it shows results similar to the topic metrics, such as TC vs ORA<sub>N</sub> as well as TD vs ORA<sub>U</sub>. Unexpectedly, GSEA exhibits the opposite of ORA when the ECR module is removed. We consider this to be because the distance between a topic and its top gene embedding is no longer constrained when the ECR component is ablated, so the set of topic-mined top genes has a much higher repetition rate, which leads to a decrease in TD and ORA<sub>U</sub>. In contrast, GSEA is analyzed for all genes, and unconstrained genes are more evenly distributed in the embedding space, at which point, although the repetition rate of each topic’s top gene set increases, the top genes occupy only a fraction of the overall genes, leading to the opposite

result being presented. This divergence highlights how interpretability metrics capture distinct aspects of biological coherence.

Removing CVE causes severe clustering degradation (ARI  $\downarrow$  7.2% and NMI  $\downarrow$  4.8%), while simple knowledge injection (w/ EC) yields marginal gains. These results confirm that the proposed cross-view distillation paradigm is essential for harmonizing external knowledge with scRNA-seq data. Besides, the foundation model scGPT underperforms in zero-shot settings (ARI  $\downarrow$  25.0% and NMI  $\downarrow$  19.8% vs. scE<sup>2</sup>TM), highlighting the need for task-specific adaptation [42].

## 2.7 Sensitivity Analysis Demonstrates the Robustness of scE<sup>2</sup>TM.

We systematically evaluate the robustness of scE<sup>2</sup>TM through comprehensive sensitivity analyses across key hyperparameters (Fig. 5). To collaborate the different perspectives, CVE mutually distills their neighborhood information. Fig. 5a exhibits stable clustering and interpretability performance for different numbers of nearest neighbors, indicating that the model is insensitive to neighborhood size selection. Next, we show how the weights of the regularization terms in ECR affect performance. The results show that as the weights increase, the performance of topics and the associated pathways for topic mining produces some changes, but remains relatively stable overall (Fig. 5b). Finally, we perform UMAP visualization on human pancreas data [43] to reveal how  $\lambda$  modulates topic-gene geometry (Fig. 5c). As the  $\mathcal{L}_{\text{ECR}}$  weights increase, we observe that the distribution between topics becomes more discrete, with genes restricted to the neighborhood of the topic. These results demonstrate scE<sup>2</sup>TM’s operational robustness while revealing fundamental regularization principles for interpretable topic modeling.

## 2.8 scE<sup>2</sup>TM Accurately Captures Underlying Biology Information in Pancreatic Data.

In this section, we demonstrate scE<sup>2</sup>TM’s biological discovery capability through comprehensive analysis of human pancreas scRNA-seq data [43]. UMAP visualization of the gene and topic embeddings learned by scE<sup>2</sup>TM shows that topics form distinct hubs surrounded by functionally related genes (Fig. 6a). Delving into the geometry of topics and their high-weight genes, Fig. 6b illustrates six representative topics and their top 5 genes according to the topic-gene matrix. The results show that closely related genes cluster tightly around the same topic, while genes associated with different topics are spatially separated. Quantitative comparisons further highlight the plausibility of the learned embeddings of scE<sup>2</sup>TM, where genes with higher weights are more similar to their corresponding topics and show a clear hierarchical relationship (Fig. 6c). We then investigate the top 10 genes for each topic mined by scE<sup>2</sup>TM and calculated the frequency of occurrence of each gene. The Supplementary Table 1 shows the 10 most frequent genes that we find have been identified experimentally or in the literature as genes that are significantly associated with the function of the pancreas or the mechanism of action of pancreatic diseases, such as INS, CEACAM7, and UCA1 [44–46].

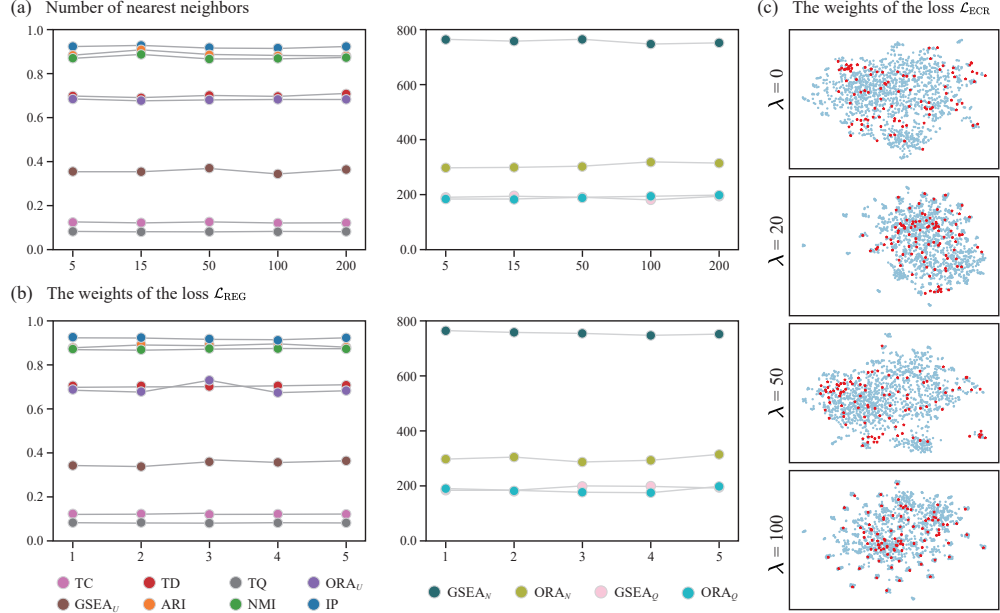


**Fig. 5** Sensitivity analysis of key hyperparameters in scE<sup>2</sup>TM. (a) Model robustness to neighborhood size in the CVE module. (b) Performance variation with different weights of loss function  $\mathcal{L}_{\text{REG}}$ . (c) Geometric evolution of topic ( $\star$ ) and gene ( $\bullet$ ) embedding space across  $\lambda$  values.

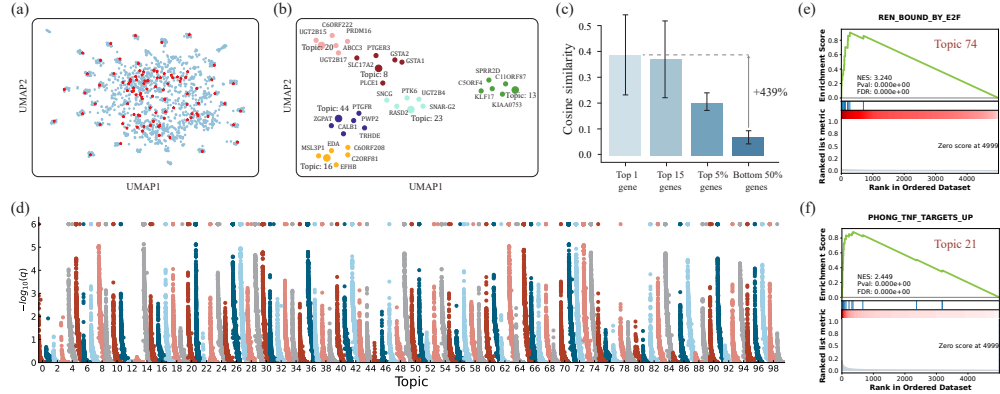


**Fig. 6** Gene set enrichment analysis (GSEA) of scE<sup>2</sup>TM on human pancreas scRNA-seq data. (a) Global distribution of genes ( $\bullet$ ) and topics ( $\star$ ) in embedding space. (b) Local topology of selected topics and their top-5 genes. Different colors distinguish different topics. (c) Similarity assessment of each topic and its top- $h$  gene. (d) Manhattan plot of GSEA results for 100 topics. The y-axis is the significance value from the permutation test corrected. (e) Leading-edge analysis of “REN\_BOUND\_BY\_E2F” pathways using Topic 74. The running sum enrichment score is calculated by GSEA. Topic 74 is significantly enriched in “REN\_BOUND\_BY\_E2F” pathway (GSEA permutation test BH adjusted  $q$ -value = 0). (f) Topic 21 is significantly enriched in “PHONG.TNF\_TARGETS.UP”.

GSEA uncovers topic-specific pathway associations with experimental support. For the human pancreas dataset, many pathways significantly enriched and closely related to pancreatic function are detected for each topic, with a Benjamin–Hochberg false discovery rate  $< 0.01$  (Fig. 6d). For instance, “REN\_BOUND\_BY\_E2F” and “SCHLOSSER\_MYC\_TARGETS\_REPRESSED\_BY\_SERUM” (Fig. 6e and Supplementary Fig. 6a) have been found to play a crucial and multifaceted role in pancreatic cells, which not only affects the normal functioning of the cells, but also influences their behavior in disease states such as diabetes and pancreatic cancer [47–49]. For “PHONG\_TNF\_TARGETS\_UP” (Fig. 6f), it has been found to play a key role in many of the deleterious effects of acute pancreatitis and to be a major determinant of the systemic progression and end-organ damage of this pathologic state [50]. Moreover, enriched “WP\_MIRNA\_TARGETS\_IN\_ECM\_AND\_MEMBRANE\_RECEPTORS” and “FOROUTAN\_INTEGRATED\_TGFB\_EMT\_DN” (Supplementary Fig. 6b and c) are well known for their significant roles in pancreatic function [51–53].

## 2.9 Complexity and Time Consumption of scE<sup>2</sup>TM is Manageable.

We benchmark computational efficiency of all models across 3 datasets of different sizes (Table 2). The results indicate that scTAG and scLEGA based on cellular networks achieve fast runtimes but prohibitively high GPU memory usage. They train the entire dataset as a whole rather than through mini-batches, which explains their short runtime. However, their whole-dataset processing design prevents scaling to large datasets. Moreover, scVI and scVI-LD show more efficient speed and resource utilization, but they have limited interpretability, which is not favorable for further analysis. In contrast, scE<sup>2</sup>TM achieves competitive efficiency while achieving strong clustering performance and interpretability, which shows that scE<sup>2</sup>TM does not significantly increase the complexity of the model, proving its scalability.

**Table 2** Efficiency analysis of different methods.

Model	Wang		Klein		Slyper	
	Runtime	Space	Runtime	Space	Runtime	Space
scVI	40s	907MB	195s	893MB	842s	897MB
scVI-LD	37s	883MB	187s	897MB	729s	873MB
scETM	140s	915MB	760s	1,167MB	4,029s	1,227MB
scTAG	44s	10,563MB	106s	10,563MB	1,439s	10,563MB
scLEGA	34s	1,093MB	167s	3,561MB	244s	6,051MB
SPRUC	119s	739MB	681s	761MB	3,391s	739MB
d-scIGM	429s	3,731MB	2,851s	3,775MB	11,154s	3,777MB
scE <sup>2</sup> TM	61s	957MB	486s	1,063MB	2,356s	1,475MB

### 3 Conclusion

With the development of deep learning-based single-cell embedding methods, there is an increasing demand for model interpretability to mine potential biological knowledge from massive scRNA-seq datasets. To bridge this gap, we develop a novel single-cell embedding topic model scE<sup>2</sup>TM and introduce 10 quantitative metrics to assess the interpretability of the model. These interpretability metrics, together with the clustering metrics, form a more comprehensive evaluation system. By comparing scE<sup>2</sup>TM with the benchmark model across multiple scRNA-seq datasets, scE<sup>2</sup>TM shows excellent interpretability and clustering performance.

In terms of integrating cell network knowledge, many existing deep learning approaches are implemented via GNNs, which substantially increases computational costs and limits scalability. In contrast, our framework leverages external knowledge from single-cell foundation models. Through a novel cross-view distillation strategy, we effectively coordinate cellular neighborhood information across different representations, achieving both superior clustering performance and enhanced scalability without incurring a computational burden similar to that of GNNs-based models.

In terms of interpretability, we introduce ECR to enhance the interpretation quality of the model. Quantitative experiments show that scE<sup>2</sup>TM’s superior interpretability over benchmark models. Qualitative experiments further demonstrate that the topic of scE<sup>2</sup>TM captures the cell functional and cell type-specific biosignals involved in single-cell data. Furthermore, by analyzing the quantitative metrics, we find that the clustering metrics and interpretability of single-cell embedded topic models are not correlated, and that several methods suffer from interpretation collapse, which lays the foundation for further improvement of the interpretation performance and understanding of the interpretation mechanism.

Future extensions of our study will focus on three directions. First, We will explore the effects of potential interpretation data selection bias, e.g., using relevant biological processes of a particular tissue or type as external interpretation data. Given the lack of relevant large-scale systematic data, in our current study it is the full range of known pathways that are explored. Nevertheless, we anticipate that diversity and consistency will remain a valid principle of assessment even on specific interpretation data. Second, in the face of the increasing amount of data, future work is needed to further improve the efficiency of scE<sup>2</sup>TM with the help of some new topic modeling strategies [54]. Finally, high-throughput assays can measure different cellular properties, including gene transcriptomes, chromatin accessibility, and so on. Topic modeling is also widely used in multimodal interpretable single-cell approaches. Therefore, we plan to further extend scE<sup>2</sup>TM and interpretable assessment metrics to multimodal single-cell data, thus enabling more comprehensive biosignal capture across modalities [55, 56].

In summary, the proposed scE<sup>2</sup>TM is an external knowledge-guided single-cell embedded topic model with powerful performance and interpretability. We point out the limitations of the current evaluation framework and further introduce a variety of interpretability quantitative metrics as a supplement. We envision that they can extend our understanding of cell biology and lay the foundation for future developments.

## 4 Methodology

### 4.1 Experiment Setup

#### 4.1.1 Datasets and Evaluation Metrics

In this study, 20 scRNA-seq datasets are used to conduct experiments, including human and mouse data. For all single-cell datasets, we perform the same preprocessing steps using Scanpy package (v.1.9.8). Specifically, we use `scanpy.pp.log1p()` to log-transform the counts of each cell, and then use `scanpy.pp.highly_variable_genes()` to pick out the top-5000 highly variable genes. Details of all single-cell data are described in Supplementary Table 2.

For cell clustering, we use representative metrics to assess the validity of our scE<sup>2</sup>TM, namely the normalized mutual information (NMI) and the adjusted rand index (ARI). All embedding maps are visualized by UMAP. We cluster the cells using Louvain’s algorithm. Furthermore, to better assess the clustering performance of cell embeddings, we experiment with multiple resolution values and reported the results with the highest ARI of each method, following previous methods [20, 57]. Last but not least, we assess model interpretability using the proposed metrics: IP, TC, TD, TQ, ORA<sub>N</sub>, ORA<sub>U</sub>, ORA<sub>Q</sub>, GSEA<sub>N</sub>, GSEA<sub>U</sub>, and GSEA<sub>Q</sub>.

#### 4.1.2 Baselines and Parameter Settings

For the single-cell embedded topic model, we use scVI-LD [58], scETM [10], SPRUCE [19], and d-scIGM [20] as our baselines. The scVI-LD method provides interpretability by determining the relationship between cell representative coordinates and gene weights through factorial modeling, where cell representative coordinates can be considered as topics. Notably, d-scIGM utilizes hierarchical prior knowledge to bootstrap the model, which may lead to a data leakage in the interpretability evaluation, so we use the version without prior knowledge mentioned in the original article. All experiments on the benchmark models are performed using publicly available code, and we use the optimal hyperparameters reported in their original papers. For models that utilize information about the topology of the cellular network, we use scTAG [32] and scLEGA [33] as baselines. In addition, scVI [59] is also used as a baseline model, which is a classical single-cell deep embedding method that has demonstrated excellent overall performance in previous comprehensive evaluations [57]. More training details of scE<sup>2</sup>TM can be found in Supplementary Note 2.

### 4.2 External Knowledge-guided Embedding Paradigm

In the pursuit of performance, a range of single-cell embedding models utilize cell expression data to construct cellular networks and use GNNs to integrate the topological information of the networks into the single-cell clustering process. Despite the progress made, this paradigm is constrained by the upper information limit of the cell expression data and the high space complexity of GNNs. In parallel, the single-cell

foundation models can provide rich external knowledge. For example, scGPT is a generative pre-trained converter trained on a database containing over 33 million cells, which provides key biological insights about genes and cells [34].

Under these considerations, we propose a new paradigm of utilizing external knowledge provided by the single-cell foundation model (i.e., scGPT), instead of using cellular networks to guide embedding representation learning. Notably, scGPT simulates the self-supervised process of large language models by the proposed “gene prompts”. By analogizing genes to words, scGPT is trained on the task of masked language model, i.e., predicting the randomly masked genes. According to the experimental results in the original paper, scGPT can capture gene granularity information well, such as the characterization of genes and the dependency information between genes. Therefore, we consider that the information extracted from scGPT and the gene expression information have certain differences in terms of information granularity and distribution, and we regard them as external and internal perspective, respectively.

The utilization of information from different perspectives or modalities is a key research direction in deep learning [60]. In the field of single-cell analysis, scNET [61] integrates both PPI networks and cellular similarity relations to learn embedded representations of genes and cells through a two-view graph neural network architecture. Tang et al. [62] propose the Monae model, a modality-specific autoencoder that exploits the regulatory relationship between RNA and ATAC modalities and employs the contrastive learning technique to enhance cellular representations in a unified space. Besides, Zhai et al. [63] design a soft-anchor-based self-supervised learning module to coordinate information in reference and target data. In this paper, we propose a cross-view distillation strategy to better reconcile scRNA-seq data with the external knowledge provided by the single cell foundation model.

Different from simply splicing cell embeddings trained on data from different perspectives, our strategy attempts to utilize the neighborhood information of the cells. The key idea of this strategy is that the same cell of different perspectives should be mapped to the same topic, and that consistent topic assignment between each cell and the corresponding neighboring cell in another perspective is encouraged to integrate the cell’s neighborhood information. Specifically, let  $\mathbf{x}$  and  $\mathbf{v}$  be the internal and external cell embedding representations, respectively. We introduce a cell-topic head  $f(\cdot) : \mathbf{x} \rightarrow \boldsymbol{\theta} \in \mathbb{R}^K$  and a cell-cluster head  $g(\cdot) : \mathbf{v} \rightarrow \boldsymbol{\varphi} \in \mathbb{R}^K$ , where  $K$  is the number of target topics/clusters<sup>1</sup>. Formally, we denote the soft topic/cluster assignment of the  $i$ -th cell as

$$\begin{aligned}\boldsymbol{\theta}_i &= f(\mathbf{x}_i) = \text{Softmax}(\text{MLP}(\mathbf{x}_i)), \\ \boldsymbol{\varphi}_i &= g(\mathbf{v}_i) = \text{Softmax}(\text{MLP}(\mathbf{v}_i)), i = 1 \dots n,\end{aligned}\tag{8}$$

where  $n$  is the number of cells.

To encourage topic consistency between internal and external perspectives of the same cell, we firstly introduce the following cross-view assignment consistency loss:

$$\mathcal{L}_{\text{CON}} = -\log \sum_{i=1}^n \boldsymbol{\theta}_i^\top \boldsymbol{\varphi}_i,\tag{9}$$

---

<sup>1</sup>It is worth noting that clusters and topics satisfy a one-to-one correspondence, and the use of different names is mainly to define the architecture of the model more clearly.

which is minimized when  $\theta_i$  and  $\varphi_i$  get close to each other.

Secondly, to utilize the cell neighborhood information of different views, we first obtain the nearest neighbors set of  $\mathbf{x}_i$  and  $\mathbf{v}_i$ , denoted as  $\mathcal{N}(\mathbf{x}_i)$  and  $\mathcal{N}(\mathbf{v}_i)$ , respectively. For randomly sampled neighbors  $\mathbf{x}_i^{\mathcal{N}} \in \mathcal{N}(\mathbf{x}_i)$  and  $\mathbf{v}_i^{\mathcal{N}} \in \mathcal{N}(\mathbf{v}_i)$ , their corresponding topic assignments are defined as

$$\theta_i^{\mathcal{N}} = f(\mathbf{x}_i^{\mathcal{N}}), \varphi_i^{\mathcal{N}} = g(\mathbf{v}_i^{\mathcal{N}}). \quad (10)$$

Let  $\theta_{ik}, \theta_{ik}^{\mathcal{N}}, \varphi_{ik}, \varphi_{ik}^{\mathcal{N}}$  be the assignment of the  $k$ -th topic/cluster, the loss function of cross-view neighborhood consistency is defined as follows:

$$\begin{aligned} \mathcal{L}_{\text{NEI}} &= \frac{1}{n} \sum_{i=1}^n \sum_{k=1}^K (L_{ik}^{\mathbf{x} \rightarrow \mathbf{v}} + L_{ik}^{\mathbf{v} \rightarrow \mathbf{x}}), \\ L_{ik}^{\mathbf{x} \rightarrow \mathbf{v}} &= -\log \frac{e^{\left(\text{sim}(\varphi_{ik}, \theta_{ik}^{\mathcal{N}})/2\right)}}{\sum_j e^{\left(\text{sim}(\varphi_{ik}, \theta_{ij}^{\mathcal{N}})/2\right)} + \sum_{j \neq i} e^{\left(\text{sim}(\varphi_{ik}, \varphi_{ij})/2\right)}}, \\ L_{ik}^{\mathbf{v} \rightarrow \mathbf{x}} &= -\log \frac{e^{\left(\text{sim}(\theta_{ik}, \varphi_{ik}^{\mathcal{N}})/2\right)}}{\sum_j e^{\left(\text{sim}(\theta_{ik}, \varphi_{ij}^{\mathcal{N}})/2\right)} + \sum_{j \neq i} e^{\left(\text{sim}(\theta_{ik}, \theta_{ij})/2\right)}}. \end{aligned} \quad (11)$$

Notably,  $\mathcal{L}_{\text{NEI}}$  encourages consistent topic assignment between a cell and its corresponding neighbor in another view, where  $L_{ik}^{\mathbf{x} \rightarrow \mathbf{v}}$  aligns the internal feature of the cell to the neighbourhood of its external features, and  $L_{ik}^{\mathbf{v} \rightarrow \mathbf{x}}$  vice versa. In addition, the second terms of the denominator in the definitions of  $L_{ik}^{\mathbf{x} \rightarrow \mathbf{v}}$  and  $L_{ik}^{\mathbf{v} \rightarrow \mathbf{x}}$  can minimize inter-topic similarity, resulting in more discriminative topics. It is worth noting that, as a classical neighbor search algorithm, the  $k$ -nearest neighbor algorithm is susceptible to “dimensionality catastrophe” and pivot effect, so we choose mutual KNN to find the set of nearest neighbors of cells [64]. In practice, we set the number of nearest neighbors  $|\mathcal{N}(\mathbf{x}_i)| = |\mathcal{N}(\mathbf{v}_i)| = 15$  ( $i = 1 \dots n$ ) for all datasets.

Thirdly, to prevent all samples from collapsing into a few topics, we introduce a regularization term to stabilize the training, i.e.,

$$\mathcal{L}_{\text{REG}} = - \sum_{i=1}^n \sum_{k=1}^K (\theta_{ik} \log \theta_{ik} + \varphi_{ik} \log \varphi_{ik}). \quad (12)$$

Finally, we derive the overall loss function of our cross-view distillation strategy as follows:

$$\mathcal{L}_{\text{CVE}} = \mathcal{L}_{\text{CON}} + \mathcal{L}_{\text{NEI}} - \alpha \cdot \mathcal{L}_{\text{REG}}, \quad (13)$$

where the weight of  $\alpha$  is set to 5.

### 4.3 Embedding Clustering Regularization

To mitigate the potential interpretation collapse problem, we extend the ECR approach of Wu et al. [29] to the single-cell domain to model the relationship between topics and genes. In our work, topics are considered as clustering centers and genes as clustering samples, so each topic should be the center of a separately aggregated gene clustering. Under this intuition, we adopt ECR to model the soft assignment of genes

to topics using a transport scheme defined specifically for the optimal transport problem. Specifically, we define two discrete measures of gene embedding  $\mathbf{g}_m$  and topic embedding  $\mathbf{t}_k$ :  $\gamma = \sum_{m=1}^V \frac{1}{V} \delta_{\mathbf{g}_m}$  and  $\phi = \sum_{k=1}^K s_k \delta_{\mathbf{t}_k}$ , where  $V$  is the number of genes and  $\delta_z$  denotes the Dirac unit mass on  $z$ . ECR formulates the entropic regularized optimal transport between  $\gamma$  and  $\phi$  as

$$\begin{aligned} \arg \min_{\pi \in \mathbb{R}_+^{V \times K}} \mathcal{L}_{\text{OT}_\varepsilon}(\gamma, \phi), \quad \mathcal{L}_{\text{OT}_\varepsilon}(\gamma, \phi) = \\ \sum_{m=1}^V \sum_{k=1}^K D(\mathbf{g}_m, \mathbf{t}_k) \pi_{mk} + \sum_{m=1}^V \sum_{k=1}^K \varepsilon \pi_{mk} (\log(\pi_{mk}) - 1) \\ \text{s.t.} \quad \pi \mathbf{1}_K = \frac{1}{V} \mathbf{1}_V \quad \text{and} \quad \pi^\top \mathbf{1}_V = \frac{1}{K} \mathbf{1}_K, \end{aligned} \quad (14)$$

where the first term is the original optimal transport problem and the second term with the hyperparameter  $\varepsilon$  is entropy regularization. Eq. (14) is to find the optimal transport plan  $\pi_\varepsilon^*$  that minimizes the total cost of transporting weight from gene embeddings to topic embeddings. We measure the transport cost between gene  $\mathbf{g}_m$  and topic  $\mathbf{t}_k$  by Euclidean distance:  $D(\mathbf{g}_m, \mathbf{t}_k) = C_{mk} = \|\mathbf{g}_m - \mathbf{t}_k\|^2$ , and the transport cost matrix is denoted as  $\mathbf{C} \in \mathbb{R}^{V \times K}$ . The two conditions in Eq. (14) restrict the weight of each gene embedding  $\mathbf{g}_m$  as  $\frac{1}{V}$  and each topic embedding  $\mathbf{t}_k$  as  $\frac{1}{K}$ , where  $\mathbf{1}_K$  ( $\mathbf{1}_V$ ) is a  $K$  ( $V$ ) dimensional column vector of ones. Besides,  $\pi_{mk}$  denotes the transport weight from  $\mathbf{g}_m$  to  $\mathbf{t}_k$  and  $\pi \in \mathbb{R}_+^{V \times K}$  is the transport plan that includes the transport weight of each gene embedding to fulfill the weight of each topic embedding. To meet the above requirements, ECR models clustering soft assignments with the optimal transport plan  $\pi_\varepsilon^*$ , i.e., the soft-assignment of  $\mathbf{g}_m$  to  $\mathbf{t}_k$  is the transport weight between them,  $\pi_{\varepsilon, mk}^*$ . The formula is defined as follows:

$$\begin{aligned} \mathcal{L}_{\text{ECR}} = \sum_{m=1}^V \sum_{k=1}^K \|\mathbf{g}_m - \mathbf{t}_k\|^2 \pi_{\varepsilon, mk}^*, \\ \text{where } \pi_\varepsilon^* = \text{sinkhorn}(\gamma, \phi, \varepsilon) \approx \arg \min_{\pi \in \mathbb{R}_+^{V \times K}} \mathcal{L}_{\text{OT}_\varepsilon}(\gamma, \phi). \end{aligned} \quad (15)$$

Sinkhorn algorithm [65] is used to compute  $\pi_\varepsilon^*$ , which can be efficiently executed on GPUs.

#### 4.4 Modeling Process

In this part, we describe the overall workflow of the proposed external knowledge-guided single-cell embedded topic model named scE<sup>2</sup>TM, as shown in Fig. 1. First of all, our model uses a Variational AutoEncode (VAE) architecture consisting of an encoder that incorporates the proposed cross-view distillation strategy and a sparse linear decoder. For parameter inference, the main loss of scE<sup>2</sup>TM is the evidence lower bound of cell reconstruction error. Moreover, to alleviate the interpretation collapse problem, we introduce the ECR module, which constrains the asymmetric dependencies between topics and genes.

#### 4.4.1 Cross-view Encoder:

The encoder of a VAE maps the input sample into the latent distribution, and we consider the distribution after reparameterization in the VAE encoder as the cell-topic distribution  $\boldsymbol{\theta}$ . On this basis, we combine the cross-view distillation strategy that we proposed above, and thus introducing external knowledge into the model to develop our cross-view encoder. Specifically, given a scRNA-seq dataset, each cell is represented as a vector  $\mathbf{x}_i \in \mathbb{R}^V$  consisting of gene expression values. The **Cross-view Encoder (CVE)** is defined as

$$\begin{aligned}\boldsymbol{\theta}_i &= f(\mathbf{x}_i) = \text{Softmax}(\text{Reparameter}(\text{MLP}(\mathbf{x}_i))), \\ \boldsymbol{\varphi}_i &= g(\mathbf{v}_i) = \text{Softmax}(\text{MLP}(\mathbf{v}_i)),\end{aligned}\tag{16}$$

where  $\mathbf{v}_i$  is the cell embedding extracted using the single-cell foundation model scGPT.  $f(\cdot)$  and  $g(\cdot)$  are the cell-topic head and cell-cluster head.

#### 4.4.2 Sparse Linear Decode:

Next, we reconstruct the input cells using the cell-topic distribution  $\boldsymbol{\theta}_i$  and gene-topic matrix  $\mathbf{O} \in \mathbb{R}^{V \times K}$ . Prior work has typically modeled  $\mathbf{O}$  as the product of topic and gene embeddings. The difference is that ECR serves as a clustering regularization of topic and gene embeddings, and  $\mathbf{O}$  needs to reflect the learned clustering distributions between them, which is defined as

$$\mathbf{O}_{mk} = \frac{e^{-\|\mathbf{g}_m - \mathbf{t}_k\|^2 / \tau}}{\sum_{j=1}^K e^{-\|\mathbf{g}_m - \mathbf{t}_j\|^2 / \tau}},\tag{17}$$

where  $\tau$  is the temperature hyperparameter. It is worth noting that ECR does not directly model  $\mathbf{O}$  with  $\pi_{\epsilon}^*$ . Thus, a gene can belong to different topics, which is consistent with reality. Finally, reconstructed cells can be periodically extracted from the multinomial distribution defined by using the cell-topic distribution matrix  $\boldsymbol{\Theta} \in \mathbb{R}^{n \times K}$  and the gene-topic distribution matrix  $\mathbf{O}$ . Formally, we have

$$\hat{\mathbf{x}} \sim \text{Multi}(\text{Softmax}(\boldsymbol{\Theta} \cdot \mathbf{O}^\top)).\tag{18}$$

#### 4.4.3 Overall Loss Function:

Similar to VAE, the loss function for cell reconstruction is defined as

$$\begin{aligned}\mathcal{L}_{\text{RE}} &= \frac{1}{n} \sum_{i=1}^n -\mathbf{x}_i^\top \log(\text{Softmax}(\boldsymbol{\theta}_i \cdot \mathbf{O}^\top)) \\ &+ \text{KL} \left[ q(\boldsymbol{\theta}_i | \mathbf{x}^{(i)}) \| p(\boldsymbol{\theta}_i) \right].\end{aligned}\tag{19}$$

The first term is the reconstruction error, and the second term is the KL divergence between the prior distribution and the variational distribution. Throughout the training process, cell embedding learning and topic modeling are co-optimized. We define

the overall loss function of scE<sup>2</sup>TM as the combination of  $\mathcal{L}_{\text{RE}}$  (Eq. (19)),  $\mathcal{L}_{\text{CVE}}$  (Eq. (13)), and  $\mathcal{L}_{\text{ECR}}$  (Eq. (15)), that is,

$$\mathcal{L} = \mathcal{L}_{\text{RE}} + \mathcal{L}_{\text{CVE}} + \lambda \cdot \mathcal{L}_{\text{ECR}}, \quad (20)$$

where  $\lambda$  is the weight hyperparameter. This overall loss function enables scE<sup>2</sup>TM to extract rich external knowledge, improve embedding quality, and avoid interpretation collapse by independent clustering centered on topic embeddings, while learning high-quality cellular embeddings and robust interpretations. Algorithm 1 (Supplementary Material) shows the training workflow of scE<sup>2</sup>TM.

## 4.5 Details of Related work

### 4.5.1 Single-cell Deep Embedding Methods

With the rapid development of deep learning, deep embedding models have been widely used in the analysis of single cells. Lopez et al. [59] propose scVI based on the VAE, which approximates the posterior distribution of scRNA-seq data through a variational inference network and reconstructs the cells using a neural decoder. Tian et al. [3] develop scDCC that combines the Zero-Inflated Negative Binomial (ZINB) model with clustering loss and constraint loss. scDHA proposed by Tran et al. [31] can utilize a non-negative kernel autoencoder to help remove genes that have little contribution to the representation of the part-based data, thus extracting representative information for each cell more accurately. However, these methods only focus on gene expression information when representing the learning process without considering the topological information of the cell network.

To naturally embed expression and relationship information into potential representations, scGNN [66] utilizes GNNs to integrate structural information of cell-cell networks. GNNs learn the representations of nodes in a graph through neighbor information propagation, taking into account both node features and graph topology. scTAG [32] uses the ZINB model as the backbone and incorporates a topologically adaptive graph convolutional autoencoder to further enhance the modeling capability. scLEGA [33] employs a novel ZINB loss function, which fully takes into account the contribution of genes with lower expression values with combines gene expression and the topological information of cellular network through a multi-point attention mechanism. Nevertheless, the large space occupation of cellular networks and graph convolution algorithms make these models difficult to scale to large single-cell datasets. In addition, these internal knowledge-based guidance paradigms are constrained by the limited information in the given data. Unlike previous approaches, we propose a new paradigm that utilizes the external knowledge obtained from the single-cell foundation model to guide single-cell embedding and clustering analysis. It is worth noting that for a more comprehensive comparison, we use the single-cell foundation model, i.e., scGPT [34], as our ablation.

### 4.5.2 Single-cell Deep Interpretable Methods

Despite the attractive performance of the deep embedding methods described above, they lack interpretability and fail to provide biologically meaningful characterization of the underlying transcriptome. The study of interpretable deep embedding models is an important direction in scRNA-seq data mining, and a series of models have been developed, which are mainly categorized into a priori knowledge-based and topic-based methods. A priori knowledge-based approach involves injecting a priori biological knowledge into the neural network architecture to improve interpretability. For instance, VEGA [67] enhances VAE with gene annotations whose decoder is a sparse single-layer neural network corresponding to a user-supplied database of gene annotations, thus providing direct interpretability of latent variables. P-NET [68] is a deep learning approach that integrates previously established knowledge of biological hierarchies into a neural network language to guide a supervised learning task, thus making predictions biologically rich and interpretable. TOSICA [69] integrates prior biological knowledge mechanisms through the mechanism of attention. However, these methods are limited by a priori information and suffer from incomplete domain knowledge and difficulty in learning new knowledge.

The single-cell embedded topic model associates topics with genes, thus providing interpretability. scETM model first [10] introduced interpretable linear decoders to learn highly interpretable gene and topic embeddings to extend topic modeling to the single-cell domain. Based on this, SPRUCE [19] combined a topic modeling approach with cell-cell interactions to simulate informational crosstalk between cell-cells while identifying cell types. Moreover, chen et al. [20] enhance the model’s ability to capture latent signals within the data by constructing deeper neural network architectures to better capture the dependencies between topics and genes. Nevertheless, existing topic-based approaches do not provide a quantitative assessment of the interpretability of the model and are not able to cope with potential interpretation collapse.

**Code Availability.** The scE<sup>2</sup>TM model and all the code necessary for reproducing our results is publicly available via GitHub at <https://github.com/nbnbhwy/scE2TM>. An archived version will be deposited in the Zenodo database upon acceptance.

**Acknowledgments.** This work is supported by the National Natural Science Foundation of China [grant number 62372483].

## References

- [1] Kolodziejczyk, A.A., Kim, J.K., Svensson, V., Marioni, J.C., Teichmann, S.A.: The technology and biology of single-cell rna sequencing. *Molecular cell* **58**(4), 610–620 (2015)
- [2] Hwang, B., Lee, J.H., Bang, D.: Single-cell rna sequencing technologies and bioinformatics pipelines. *Experimental & molecular medicine* **50**(8), 1–14 (2018)

- [3] Tian, T., Zhang, J., Lin, X., Wei, Z., Hakonarson, H.: Model-based deep embedding for constrained clustering analysis of single cell rna-seq data. *Nature communications* **12**(1), 1873 (2021)
- [4] Ma, Q., Xu, D.: Deep learning shapes single-cell data analysis. *Nature Reviews Molecular Cell Biology* **23**(5), 303–304 (2022)
- [5] Rudin, C.: Stop explaining black box machine learning models for high stakes decisions and use interpretable models instead. *Nature Machine Intelligence* **1**(5), 206–215 (2019)
- [6] Klauschen, F., Dippel, J., Keyl, P., Jurmeister, P., Bockmayr, M., Mock, A., Buchstab, O., Alber, M., Ruff, L., Montavon, G., *et al.*: Toward explainable artificial intelligence for precision pathology. *Annual Review of Pathology: Mechanisms of Disease* **19**(1), 541–570 (2024)
- [7] Lundberg, S.M., Lee, S.-I.: A unified approach to interpreting model predictions. In: *NeurIPS*, pp. 4765–4774 (2017)
- [8] Tseng, A., Shrikumar, A., Kundaje, A.: Fourier-transform-based attribution priors improve the interpretability and stability of deep learning models for genomics. In: *NeurIPS*, pp. 1913–1923 (2020)
- [9] Tao, Y., Ma, X., Palmer, D., Schwartz, R., Lu, X., Osmanbeyoglu, H.U.: Interpretable deep learning for chromatin-informed inference of transcriptional programs driven by somatic alterations across cancers. *Nucleic Acids Research* **50**(19), 10869–10881 (2022)
- [10] Zhao, Y., Cai, H., Zhang, Z., Tang, J., Li, Y.: Learning interpretable cellular and gene signature embeddings from single-cell transcriptomic data. *Nature communications* **12**(1), 5261 (2021)
- [11] Li, Y., Yang, A.Y., Marelli, A., Li, Y.: Mixehr-surg: A joint proportional hazard and guided topic model for inferring mortality-associated topics from electronic health records. *Journal of Biomedical Informatics* **153**, 104638 (2024)
- [12] Li, Y., Nair, P., Lu, X.H., Wen, Z., Wang, Y., Dehaghi, A.A.K., Miao, Y., Liu, W., Ordog, T., Biernacka, J.M., *et al.*: Inferring multimodal latent topics from electronic health records. *Nature communications* **11**(1), 2536 (2020)
- [13] Chen, H., Mao, P., Lu, Y., Rao, Y.: Nonlinear structural equation model guided gaussian mixture hierarchical topic modeling. In: *ACL*, pp. 10377–10390 (2023)
- [14] Lu, Y., Chen, H., Mao, P., Rao, Y., Xie, H., Wang, F.L., Li, Q.: Self-supervised topic taxonomy discovery in the box embedding space. *Transactions of the Association for Computational Linguistics* **12**, 1401–1416 (2024)

- [15] Nguyen, T.T., Wu, X., Dong, X., Nguyen, C.T., Ng, S., Luu, A.T.: Topic modeling as multi-objective contrastive optimization. In: ICLR (2024)
- [16] Chen, R., Chen, H., Lu, Y., Rao, Y., Zhu, C.: Supervised neural topic modeling with label alignment. *Transactions of the Association for Computational Linguistics* **13**, 249–263 (2025)
- [17] Lynch, A.W., Theodoris, C.V., Long, H.W., Brown, M., Liu, X.S., Meyer, C.A.: Mira: joint regulatory modeling of multimodal expression and chromatin accessibility in single cells. *Nature methods* **19**(9), 1097–1108 (2022)
- [18] Zhang, Y., Khalilitousi, M.S., Park, Y.P.: Unraveling dynamically encoded latent transcriptomic patterns in pancreatic cancer cells by topic modeling. *Cell Genomics* **3**(9) (2023)
- [19] Subedi, S., Park, Y.P.: Single-cell pair-wise relationships untangled by composite embedding model. *Iscience* **26**(2) (2023)
- [20] Chen, H., Lu, Y., Dai, Z., Yang, Y., Li, Q., Rao, Y.: Comprehensive single-cell rna-seq analysis using deep interpretable generative modeling guided by biological hierarchy knowledge. *Briefings in Bioinformatics* **25**(4), 314 (2024)
- [21] Kazwini, N.E., Sanguinetti, G.: Share-topic: Bayesian interpretable modeling of single-cell multi-omic data. *Genome Biology* **25**(1), 55 (2024)
- [22] Fan, Y., Li, Y., Ding, J., Li, Y.: Gfetm: Genome foundation-based embedded topic model for scatac-seq modeling. In: *International Conference on Research in Computational Molecular Biology*, pp. 314–319 (2024). Springer
- [23] Zhong, C., Ang, K.S., Chen, J.: Interpretable spatially aware dimension reduction of spatial transcriptomics with stamp. *Nature Methods*, 1–12 (2024)
- [24] Srivastava, A., Sutton, C.: Autoencoding variational inference for topic models. *arXiv preprint arXiv:1703.01488* (2017)
- [25] Zhao, H., Phung, D., Huynh, V., Le, T., Buntine, W.: Neural topic model via optimal transport. In: ICLR (2021)
- [26] Rudin, C., Chen, C., Chen, Z., Huang, H., Semenova, L., Zhong, C.: Interpretable machine learning: Fundamental principles and 10 grand challenges. *Statistic Surveys* **16**, 1–85 (2022)
- [27] Chen, V., Yang, M., Cui, W., Kim, J.S., Talwalkar, A., Ma, J.: Applying interpretable machine learning in computational biology—pitfalls, recommendations and opportunities for new developments. *Nature Methods* **21**(8), 1454–1461 (2024)
- [28] Wagle, M.M., Long, S., Chen, C., Liu, C., Yang, P.: Interpretable deep learning

in single-cell omics. *Bioinformatics*, 374 (2024)

- [29] Wu, X., Dong, X., Nguyen, T.T., Luu, A.T.: Effective neural topic modeling with embedding clustering regularization. In: *ICML*, pp. 37335–37357 (2023). PMLR
- [30] Andreatta, M., Carmona, S.J.: Ucell: Robust and scalable single-cell gene signature scoring. *Computational and structural biotechnology journal* **19**, 3796–3798 (2021)
- [31] Tran, D., Nguyen, H., Tran, B., La Vecchia, C., Luu, H.N., Nguyen, T.: Fast and precise single-cell data analysis using a hierarchical autoencoder. *Nature communications* **12**(1), 1029 (2021)
- [32] Yu, Z., Lu, Y., Wang, Y., Tang, F., Wong, K.-C., Li, X.: Zinb-based graph embedding autoencoder for single-cell rna-seq interpretations. In: *AAAI*, vol. 36, pp. 4671–4679 (2022)
- [33] Liu, Z., Liang, Y., Wang, G., Zhang, T.: sclega: an attention-based deep clustering method with a tendency for low expression of genes on single-cell rna-seq data. *Briefings in Bioinformatics* **25**(5), 371 (2024)
- [34] Cui, H., Wang, C., Maan, H., Pang, K., Luo, F., Duan, N., Wang, B.: scgpt: toward building a foundation model for single-cell multi-omics using generative ai. *Nature Methods* **21**, 1470–1480 (2024)
- [35] Hao, M., Gong, J., Zeng, X., Liu, C., Guo, Y., Cheng, X., Wang, T., Ma, J., Zhang, X., Song, L.: Large-scale foundation model on single-cell transcriptomics. *Nature Methods* **21**, 1481–1491 (2024)
- [36] Bravo González-Blas, C., De Winter, S., Hulselmans, G., Hecker, N., Matetovici, I., Christiaens, V., Poovathingal, S., Wouters, J., Aibar, S., Aerts, S.: Scenic+: single-cell multiomic inference of enhancers and gene regulatory networks. *Nature Methods* **20**(9), 1355–1367 (2023)
- [37] Zhou, M., Zhang, H., Bai, Z., Mann-Krzisnik, D., Wang, F., Li, Y.: Single-cell multi-omics topic embedding reveals cell-type-specific and covid-19 severity-related immune signatures. *Cell Reports Methods* **3**(8) (2023)
- [38] Wallach, H., Mimno, D., McCallum, A.: Rethinking lda: Why priors matter. *Advances in neural information processing systems* **22** (2009)
- [39] Lau, J.H., Newman, D., Baldwin, T.: Machine reading tea leaves: Automatically evaluating topic coherence and topic model quality. In: *NAACL*, pp. 530–539 (2014)
- [40] Gillespie, M., Jassal, B., Stephan, R., Milacic, M., Rothfels, K., Senff-Ribeiro, A., Griss, J., Sevilla, C., Matthews, L., Gong, C., *et al.*: The reactome pathway

- knowledgebase 2022. Nucleic acids research **50**(D1), 687–692 (2022)
- [41] Lin, Z., Chen, H., Lu, Y., Rao, Y., Xu, H., Lai, H.: Hierarchical topic modeling via contrastive learning and hyperbolic embedding. In: COLING, pp. 8133–8143 (2024)
  - [42] Kedzierska, K.Z., Crawford, L., Amini, A.P., Lu, A.X.: Assessing the limits of zero-shot foundation models in single-cell biology. *bioRxiv*, 2023–10 (2023)
  - [43] Wang, Y.J., Schug, J., Won, K.-J., Liu, C., Naji, A., Avrahami, D., Golson, M.L., Kaestner, K.H.: Single-cell transcriptomics of the human endocrine pancreas. *Diabetes* **65**(10), 3028–3038 (2016)
  - [44] Andrali, S.S., Sampley, M.L., Vanderford, N.L., Özcan, S.: Glucose regulation of insulin gene expression in pancreatic  $\beta$ -cells. *Biochemical Journal* **415**(1), 1–10 (2008)
  - [45] Raj, D., Nikolaidi, M., Garces, I., Lorizio, D., Castro, N.M., Caiafa, S.G., Moore, K., Brown, N.F., Kocher, H.M., Duan, X., *et al.*: Ceacam7 is an effective target for car t-cell therapy of pancreatic ductal adenocarcinoma. *Clinical Cancer Research* **27**(5), 1538–1552 (2021)
  - [46] Chen, P., Wan, D., Zheng, D., Zheng, Q., Wu, F., Zhi, Q.: Long non-coding rna uca1 promotes the tumorigenesis in pancreatic cancer. *Biomedicine & pharmacotherapy* **83**, 1220–1226 (2016)
  - [47] Bertonnier-Brouty, L., Andersson, J., Kaprio, T., Hagström, J., Bsharat, S., Asplund, O., Hatem, G., Haglund, C., Seppänen, H., Prasad, R.B., *et al.*: E2f transcription factors promote tumorigenicity in pancreatic ductal adenocarcinoma. *Cancer medicine* **13**(9), 7187 (2024)
  - [48] Iglesias, A., Murga, M., Laresgoiti, U., Skoudy, A., Bernales, I., Fullaondo, A., Moreno, B., Lloreta, J., Field, S.J., Real, F.X., *et al.*: Diabetes and exocrine pancreatic insufficiency in e2f1/e2f2 double-mutant mice. *The Journal of clinical investigation* **113**(10), 1398–1407 (2004)
  - [49] Rosselot, C., Baumel-Alterzon, S., Li, Y., Brill, G., Lambertini, L., Katz, L.S., Lu, G., Garcia-Ocaña, A., Scott, D.K.: The many lives of myc in the pancreatic  $\beta$ -cell. *Journal of Biological Chemistry* **296** (2021)
  - [50] Malleo, G., Mazzon, E., Siriwardena, A.K., Cuzzocrea, S.: Tnf- $\alpha$  as a therapeutic target in acute pancreatitis—lessons from experimental models. *The Scientific World Journal* **7**(1), 431–448 (2007)
  - [51] Ferrara, B., Pignatelli, C., Cossutta, M., Citro, A., Courty, J., Piemonti, L.: The extracellular matrix in pancreatic cancer: description of a complex network and promising therapeutic options. *Cancers* **13**(17), 4442 (2021)

- [52] Weniger, M., Honselmann, K.C., Liss, A.S.: The extracellular matrix and pancreatic cancer: a complex relationship. *Cancers* **10**(9), 316 (2018)
- [53] Principe, D.R., Timbers, K.E., Atia, L.G., Koch, R.M., Rana, A.: Tgf $\beta$  signaling in the pancreatic tumor microenvironment. *Cancers* **13**(20), 5086 (2021)
- [54] Wu, X., Nguyen, T.T., Zhang, D.C., Wang, W.Y., Luu, A.T.: Fastopic: Pretrained transformer is a fast, adaptive, stable, and transferable topic model. In: *NeurIPS* (2024)
- [55] Coleman, K., Schroeder, A., Loth, M., Zhang, D., Park, J.H., Sung, J.-Y., Blank, N., Cowan, A.J., Qian, X., Chen, J., et al.: Resolving tissue complexity by multimodal spatial omics modeling with miso. *Nature methods*, 1–9 (2025)
- [56] Cui, H., Tejada-Lapueta, A., Brbić, M., Saez-Rodriguez, J., Cristea, S., Goodarzi, H., Lotfollahi, M., Theis, F.J., Wang, B.: Towards multimodal foundation models in molecular cell biology. *Nature* **640**(8059), 623–633 (2025)
- [57] Luecken, M.D., Büttner, M., Chaichoompu, K., Danese, A., Interlandi, M., Müller, M.F., Strobl, D.C., Zappia, L., Dugas, M., Colomé-Tatché, M., et al.: Benchmarking atlas-level data integration in single-cell genomics. *Nature Methods* **19**(1), 41–50 (2022)
- [58] Svensson, V., Gayoso, A., Yosef, N., Pachter, L.: Interpretable factor models of single-cell rna-seq via variational autoencoders. *Bioinformatics* **36**(11), 3418–3421 (2020)
- [59] Lopez, R., Regier, J., Cole, M.B., Jordan, M.I., Yosef, N.: Deep generative modeling for single-cell transcriptomics. *Nature methods* **15**(12), 1053 (2018)
- [60] Li, Y., Hu, P., Peng, D., Lv, J., Fan, J., Peng, X.: Image clustering with external guidance. In: *ICML* (2024)
- [61] Sheinin, R., Sharan, R., Madi, A.: scnet: learning context-specific gene and cell embeddings by integrating single-cell gene expression data with protein–protein interactions. *Nature Methods*, 1–9 (2025)
- [62] Tang, Z., Chen, G., Chen, S., Yao, J., You, L., Chen, C.Y.-C.: Modal-nexus auto-encoder for multi-modality cellular data integration and imputation. *Nature Communications* **15**(1), 9021 (2024)
- [63] Zhai, Y., Chen, L., Deng, M.: Generalized cell type annotation and discovery for single-cell rna-seq data. In: *AAAI*, vol. 37, pp. 5402–5410 (2023)
- [64] Dalmia, A., Sia, S.: Clustering with umap: Why and how connectivity matters. *arXiv preprint arXiv:2108.05525* (2021)
- [65] Cuturi, M.: Sinkhorn distances: Lightspeed computation of optimal transport. In:

- Burges, C.J.C., Bottou, L., Ghahramani, Z., Weinberger, K.Q. (eds.) NeurIPS, pp. 2292–2300 (2013)
- [66] Wang, J., Ma, A., Chang, Y., Gong, J., Jiang, Y., Qi, R., Wang, C., Fu, H., Ma, Q., Xu, D.: scgcn is a novel graph neural network framework for single-cell rna-seq analyses. *Nature communications* **12**(1), 1882 (2021)
  - [67] Seninge, L., Anastopoulos, I., Ding, H., Stuart, J.: Vega is an interpretable generative model for inferring biological network activity in single-cell transcriptomics. *Nature communications* **12**(1), 5684 (2021)
  - [68] Elmarakeby, H.A., Hwang, J., Arafteh, R., Crowdis, J., Gang, S., Liu, D., AlDubayan, S.H., Salari, K., Kregel, S., Richter, C., *et al.*: Biologically informed deep neural network for prostate cancer discovery. *Nature* **598**(7880), 348–352 (2021)
  - [69] Chen, J., Xu, H., Tao, W., Chen, Z., Zhao, Y., Han, J.-D.J.: Transformer for one stop interpretable cell type annotation. *Nature Communications* **14**(1), 223 (2023)

# scE<sup>2</sup>TM: Toward Interpretable Single-Cell Embedding via Topic Modeling

Hegang Chen<sup>1</sup>, Yuyin Lu<sup>1</sup>, Zhiming Dai<sup>1</sup>, Fu Lee Wang<sup>2</sup>,  
Qing Li<sup>3</sup>, Yanghui Rao<sup>1\*</sup>

<sup>1</sup>\*School of Computer Science and Engineering, Sun Yat-sen University,  
132 Waihuan East Road, Guangzhou, 510006, China.

<sup>2</sup>School of Science and Technology, Hong Kong Metropolitan  
University, Mong Man Wai Building, Hong Kong, 999077, China.

<sup>3</sup>Department of Computing, The Hong Kong Polytechnic University,  
Street, Hong Kong, 610101, China.

\*Corresponding author(s). E-mail(s): [raoyangh@mail.sysu.edu.cn](mailto:raoyangh@mail.sysu.edu.cn);  
Contributing authors: [chenhg25@mail2.sysu.edu.cn](mailto:chenhg25@mail2.sysu.edu.cn);  
[luyy37@mail2.sysu.edu.cn](mailto:luyy37@mail2.sysu.edu.cn); [daizhim@mail.sysu.edu.cn](mailto:daizhim@mail.sysu.edu.cn);  
[pwang@hkmu.edu.hk](mailto:pwang@hkmu.edu.hk); [csqli@comp.polyu.edu.hk](mailto:csqli@comp.polyu.edu.hk);

**Supplementary Information includes:**

**Supplementary Notes 1 to 2.**

**Supplementary Figures 1 to 6.**

**Supplementary Tables 1 to 2.**

# 1 Supplementary Notes

## Supplementary Note 1: Topic Enrichment Analysis

To assess whether a topic is enriched in any known pathways, a common approach is to detect over-representation analysis (ORA) [1] and Gene Set Enrichment Analysis (GSEA) [2]. ORA contains a background gene set (with known gene functions or pathways) and a specific gene set, and determines whether a specific gene set is enriched for the pathway by identifying the specific gene set as containing a higher proportion of genes than the background gene set, where the specific gene set is selected based on a threshold value. GSEA avoids threshold selection by calculating running sums of enrichment scores down the list of genes, and is one of the commonly used methods for pathway enrichment analysis. There are three key elements of the GSEA method. 1) An enrichment score is computed, which reflects the extent to which the pathway set  $S$  is overrepresented at the extremes (top or bottom) of the entire ranked list. 2) Estimate the statistical significance of enrichment score by using an empirical phenotype-based permutation testing program. 3) When evaluating the entire gene set database, we adjusted the estimated significance level to account for multiple hypothesis testing.

In this study, the top-10 genes per topic are used for calculating the topics as well as the metrics for the topic ORA analysis. For the calculation of TCs, we used as external corpus all known gene pathways (msigdb.v2024.1.Hs.symbols and msigdb.v2024.1.Mm.symbols) for mouse and human, respectively, which are downloaded from the GSEA database (<https://www.gsea-msigdb.org/>). Moreover, when performing ORA and GSEA, the external genes we used are curated gene sets from GSEA for humans and mouse.

## Supplementary Note 2: Training Details

Our scE<sup>2</sup>TM is implemented in Python and the core model is based on the Pytorch (v.1.9.8) framework. Throughout the training process, we set the dimension size of each hidden layer to 200 and use Tanh() as the activation function. The optimization of scE<sup>2</sup>TM is performed using the RMSprop optimizer with 500 iterations. For datasets with more than 10,000 cells, we uniformly use a batch size of 2048, otherwise it is set to 512. For  $\lambda$ , following the setup of Wu et al. [3], its value is set to 20 or 100 for different datasets. Furthermore, for better comparison, we follow previous work [4, 5] in setting the number of topics  $K$  to 100 for all single-cell embedded topic models. When calculating TC, TD, TQ, ORA<sub>N</sub>, ORA<sub>U</sub>, and ORA<sub>Q</sub>, we set the number of representative genes  $h$  of the topics to 10, a value that is frequently used for topic modeling. All experiments, except for the embedding extraction of the foundation model, are conducted in a Python environment equipped with an Nvidia RTX 3090 GPU and 128G RAM.

## 2 Supplementary Figures

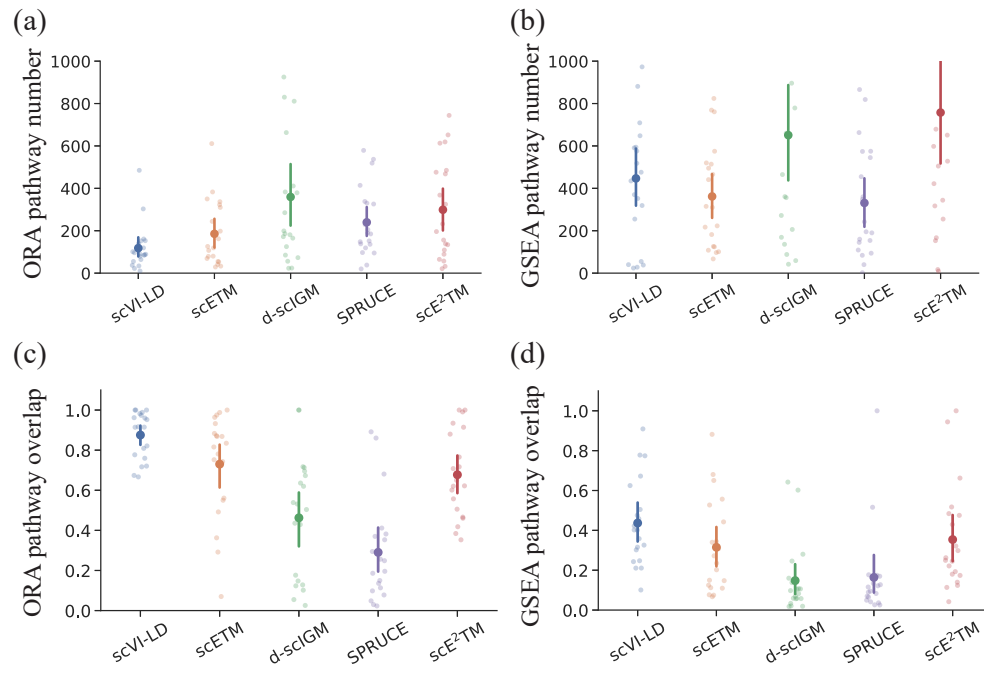


**Fig. 1** The interpretability evaluation of single-cell embedded topic models.

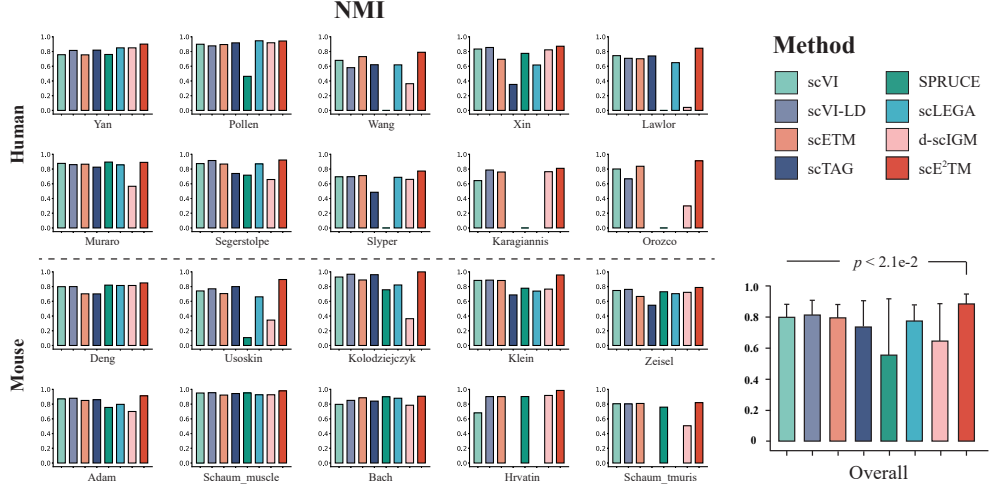


**Fig. 2** Evaluating clustering performance with NMI. The 20 panels on the left show the NMI values for the different methods on individual dataset, and the right panel shows the average NMI values and standard deviations, with statistical significance tested by pairwise Whitman U-test. We do not report the results of scTAG and scLEGA on some large scRNA-seq datasets (Karagiannis, Orozco, Hrvatin, and Schaum\_tmuris) because they are out of memory.

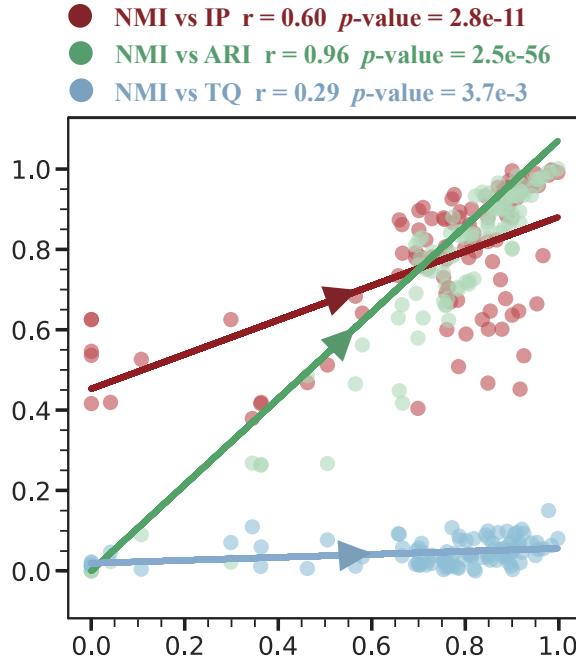


**Fig. 3** Evaluation of the correlation between the clustering metric NMI and IP, ARI and TQ.

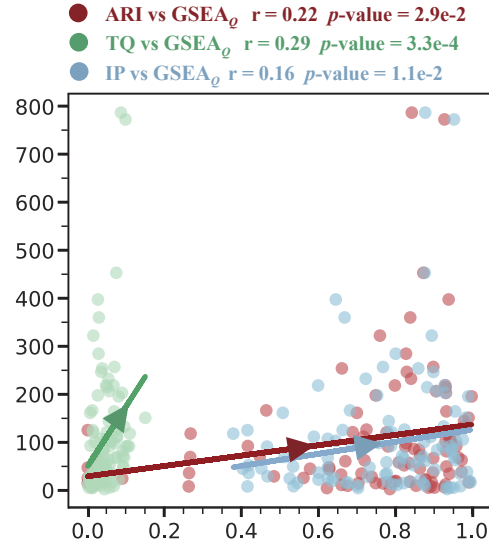


**Fig. 4** Evaluation of the correlation between topic gene set enrichment analysis quality GSEA<sub>Q</sub> and ARI, TQ and IP.

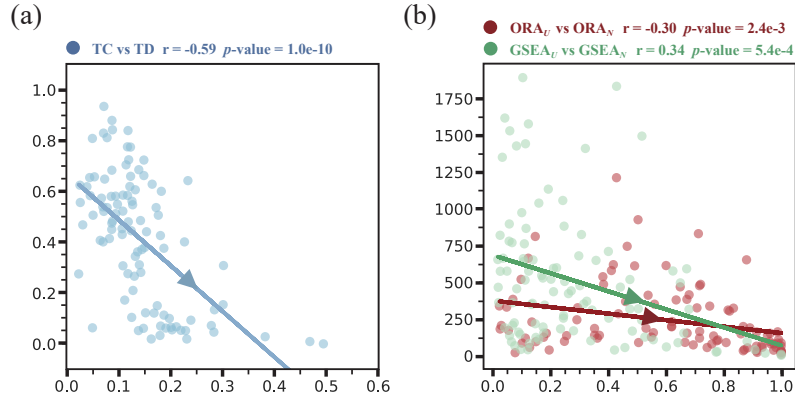


**Fig. 5** Assessment of the correlation of different metrics.

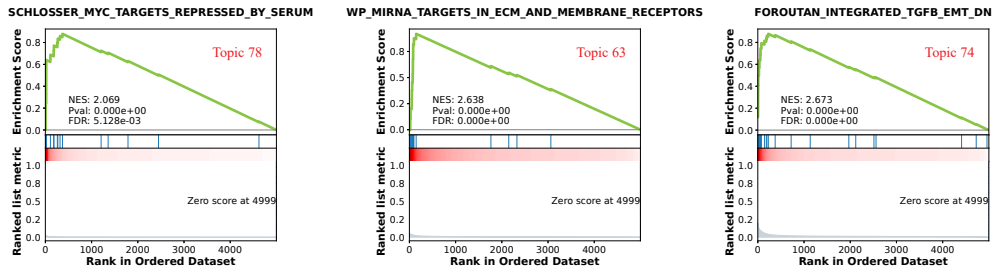


**Fig. 6** Gene set enrichment analysis of topics mined by scE<sup>2</sup>TM on human pancreas dataset (Wang).

### 3 Supplementary Tables

**Table 1** A total of 10 predictions ( 100% success rate) have been validated by previously reported experimental data. Type “a” indicates experimental data. type “NA”: There is no available literature for this prediction.

Index	Gene_name	Gene_stable_ID	Type	Reference
1	INS	ENSG00000254647	a	Andrali et al., 2008 [6]
2	CEACAM7	ENSG00000007306	a	Raj et al., 2021 [7]
3	UCA1	ENSG00000214049	a	Chen et al., 2016 [8]
4	LCN2	ENSG00000148346	a	Gumpper et al., 2020 [9]
5	PCSK1	ENSG00000175426	a	Wang et al., 2024 [10]
6	SAA2	ENSG00000134339	a	Chen et al., 2025 [11]
7	RBP4	ENSG00000138207	a	Fan et al., 2024 [12]
8	GCG	ENSG00000115263	a	Miyazaki et al., 2021 [13]
9	PENK	ENSG00000181195	a	Jin et al., 2018 [14]
10	NPY	ENSG00000122585	a	Myrsen-Axcrona et al., 1997 [15]

**Table 2** The statistics of datasets.

Dataset	Tissue	#Sample size	#Class	Protocol	Accession ID	Reference
Yan	Human embryo	90	6	Tang	GSE36552	Yan et al. [16]
Deng	Mouse embryo	268	6	Smart-Seq2	GSE45719	Deng et al. [17]
Pollen	Human brain	301	11	SMARTer	SRP041736	Pollen et al. [18]
Wang	Human pancreas	457	7	SMARTer	GSE83139	Wang et al. [19]
Lawlor	Human pancreas	604	9	SMARTer	GSE86473	Lawlor et al. [20]
Usoskin	Mouse brain	622	4	STRT-Seq	GSE59739	Usoskin et al. [21]
Kolodziejczyk	Mouse embryo stem cells	704	3	SMARTer	E-MTAB-2600	Kolodziejczyk et al. [22]
Xin	Human pancreas	1,600	8	SMARTer	GSE81608	Xin et al. [23]
Muraro	Human pancreas	2,126	10	CEL-Seq2	GSE85241	Muraro et al. [24]
Segerstolpe	Human pancreas	2,209	14	Smart-Seq2	E-MTAB-5061	Segerstolpe et al. [25]
Klein	Mouse embryo stem cells	2,717	4	inDrop	GSE65525	Klein et al. [26]
Zeisel	Mouse brain	3,005	9	STRT-Seq	GSE60361	Zeisel et al. [27]
Adam	Mouse kidney	3,660	8	Drop-seq	GSE94333	Adam et al. [28]
Schaum_muscle	Mouse limb muscle	3,909	6	10X Genomics	GSE109774	Schaum et al. [29]
Slyper	Human blood	13,316	8	10X Genomics	SCP345	Single Cell Portal [30]
Bach	Mouse mammary epithelial cells	23,184	8	10X Genomics	GSE106273	Bach et al. [31]
Hrvatin	Mouse visual cortex	48,266	8	inDrop	GSE102827	Hrvatin et al. [32]
Schaum_tmuris	Mouse tissues	54,439	40	10X genomics	GSE109774	Schaum et al. [29]
Karagiannis	Human blood	72,914	12	10X genomics	GSE128879	Karagiannis et al. [33]
Orozco	Human eye	100,055	11	10X genomics	GSE135133	Orozco et al. [34]

---

**Algorithm 1** Training algorithm for scE<sup>2</sup>TM

---

**Input:** expression feature of cells  $\mathbf{X} = \{\mathbf{x}_i\}$ ; cell embeddings from scGPT  $\mathbf{V} = \{\mathbf{v}_i\}$ .

**Hyperparameter:** number of epochs  $n_e$ ; weight of the ECR loss  $\lambda$ .

**Output:** topic embeddings  $\mathbf{T} = \{\mathbf{t}_k\}$ ; gene embeddings  $\mathbf{G} = \{\mathbf{g}_m\}$ ; cell-topic matrix  $\Theta = \{\theta_i\}$ ; gene-topic distributions  $\mathbf{O}$ .

```
1: for 1 to  $n_e$  do
2:   for each mini-batch from  $\mathbf{X}$  and  $\mathbf{V}$  do
3:      $\theta_i, \varphi_i \leftarrow \text{Encode}(\mathbf{x}_i, \mathbf{v}_i)$   $\triangleright$  Cross-view encoder
4:     Compute  $\mathbf{O}$  by Eq. (10)
5:      $\hat{\mathbf{x}}_i \leftarrow \text{Decode}(\theta_i, \mathbf{O})$   $\triangleright$  Sparse linear decoder
6:     Compute  $\mathcal{L}_{\text{RE}}$  by Eq. (12)
7:      $\triangleright$  CVE
8:     Sample neighbors  $\mathbf{x}_i^{\mathcal{N}} \in \mathcal{N}(\mathbf{x}_i)$  and  $\mathbf{v}_i^{\mathcal{N}} \in \mathcal{N}(\mathbf{v}_i)$ 
9:      $\theta_i^{\mathcal{N}}, \varphi_i^{\mathcal{N}} \leftarrow \text{Encode}(\mathbf{x}_i^{\mathcal{N}}, \mathbf{v}_i^{\mathcal{N}})$   $\triangleright$  Cross-view encoder
10:    Compute  $\mathcal{L}_{\text{CVE}}$  by Eq. (6)
11:     $\triangleright$  ECR
12:     $C_{mk} = \|\mathbf{g}_m - \mathbf{t}_k\|^2, \forall m, k$ 
13:     $\pi_\epsilon^* \leftarrow \text{Sinkhorn}(\mathbf{C})$ 
14:    Compute  $\mathcal{L}_{\text{ECR}}$  by Eq. (8)
15:     $\triangleright$  Parameter Inference
16:    Compute  $\mathcal{L} = \mathcal{L}_{\text{RE}} + \mathcal{L}_{\text{CVE}} + \lambda \cdot \mathcal{L}_{\text{ECR}}$ 
17:    Update  $\mathbf{T}, \mathbf{G}, \Theta, \mathbf{O}$  with a gradient step
```

---

## References

- [1] Boyle, E.I., Weng, S., Gollub, J., Jin, H., Botstein, D., Cherry, J.M., Sherlock, G.: Go:: Termfinder—open source software for accessing gene ontology information and finding significantly enriched gene ontology terms associated with a list of genes. *Bioinformatics* **20**(18), 3710–3715 (2004)
- [2] Subramanian, A., Tamayo, P., Mootha, V.K., Mukherjee, S., Ebert, B.L., Gillette, M.A., Paulovich, A., Pomeroy, S.L., Golub, T.R., Lander, E.S., *et al.*: Gene set enrichment analysis: a knowledge-based approach for interpreting genome-wide expression profiles. *Proceedings of the National Academy of Sciences* **102**(43), 15545–15550 (2005)
- [3] Wu, X., Dong, X., Nguyen, T.T., Luu, A.T.: Effective neural topic modeling with embedding clustering regularization. In: *ICML*, pp. 37335–37357 (2023). PMLR
- [4] Zhao, Y., Cai, H., Zhang, Z., Tang, J., Li, Y.: Learning interpretable cellular and gene signature embeddings from single-cell transcriptomic data. *Nature communications* **12**(1), 5261 (2021)
- [5] Chen, H., Lu, Y., Dai, Z., Yang, Y., Li, Q., Rao, Y.: Comprehensive single-cell rna-seq analysis using deep interpretable generative modeling guided by biological

hierarchy knowledge. *Briefings in Bioinformatics* **25**(4), 314 (2024)

- [6] Andrali, S.S., Sampley, M.L., Vanderford, N.L., Özcan, S.: Glucose regulation of insulin gene expression in pancreatic  $\beta$ -cells. *Biochemical Journal* **415**(1), 1–10 (2008)
- [7] Raj, D., Nikolaidi, M., Garces, I., Lorizio, D., Castro, N.M., Caiafa, S.G., Moore, K., Brown, N.F., Kocher, H.M., Duan, X., *et al.*: Ceacam7 is an effective target for car t-cell therapy of pancreatic ductal adenocarcinoma. *Clinical Cancer Research* **27**(5), 1538–1552 (2021)
- [8] Chen, P., Wan, D., Zheng, D., Zheng, Q., Wu, F., Zhi, Q.: Long non-coding rna ucal promotes the tumorigenesis in pancreatic cancer. *Biomedicine & pharmacotherapy* **83**, 1220–1226 (2016)
- [9] Gumpfer, K., Dangel, A.W., Pita-Grisanti, V., Krishna, S.G., Lara, L.F., Mace, T., Papachristou, G.I., Conwell, D.L., Hart, P.A., Cruz-Monserrate, Z.: Lipocalin-2 expression and function in pancreatic diseases. *Pancreatology* **20**(3), 419–424 (2020)
- [10] Wang, L., Baek, S., Prasad, G., Wildenthal, J., Guo, K., Sturgill, D., Truongvo, T., Char, E., Pegoraro, G., McKinnon, K., *et al.*: Predictive prioritization of enhancers associated with pancreas disease risk. *bioRxiv* (2024)
- [11] Chen, Y., Shi, H., Xu, Y., Zhuo, Z.: Decoding the pro-invasive role of saa2 in renal cell carcinoma: an exploratory study and experimental validation. *American Journal of Clinical and Experimental Urology* **13**(2), 132 (2025)
- [12] Fan, J., Hu, J.: Retinol binding protein 4 and type 2 diabetes: from insulin resistance to pancreatic  $\beta$ -cell function. *Endocrine* **85**(3), 1020–1034 (2024)
- [13] Miyazaki, S., Tashiro, F., Tsuchiya, T., Sasaki, K., Miyazaki, J.-i.: Establishment of a long-term stable  $\beta$ -cell line and its application to analyze the effect of gcg expression on insulin secretion. *Scientific Reports* **11**(1), 477 (2021)
- [14] Jin, T., Hao, J., Fan, D.: Nicotine induces aberrant hypermethylation of tumor suppressor genes in pancreatic epithelial ductal cells. *Biochemical and Biophysical Research Communications* **499**(4), 934–940 (2018)
- [15] Myrsen-Axcrona, U., Ekblad, E., Sundler, F.: Developmental expression of npy, ppy and pp in the rat pancreas and their coexistence with islet hormones. *Regulatory peptides* **68**(3), 165–175 (1997)
- [16] Yan, L., Yang, M., Guo, H., Yang, L., Wu, J., Li, R., Liu, P., Lian, Y., Zheng, X., Yan, J., *et al.*: Single-cell rna-seq profiling of human preimplantation embryos and embryonic stem cells. *Nature structural & molecular biology* **20**(9), 1131–1139 (2013)

- [17] Deng, Q., Ramsköld, D., Reinius, B., Sandberg, R.: Single-cell rna-seq reveals dynamic, random monoallelic gene expression in mammalian cells. *Science* **343**(6167), 193–196 (2014)
- [18] Pollen, A.A., Nowakowski, T.J., Shuga, J., Wang, X., Leyrat, A.A., Lui, J.H., Li, N., Szpankowski, L., Fowler, B., Chen, P., *et al.*: Low-coverage single-cell mrna sequencing reveals cellular heterogeneity and activated signaling pathways in developing cerebral cortex. *Nature biotechnology* **32**(10), 1053–1058 (2014)
- [19] Wang, Y.J., Schug, J., Won, K.-J., Liu, C., Naji, A., Avrahami, D., Golson, M.L., Kaestner, K.H.: Single-cell transcriptomics of the human endocrine pancreas. *Diabetes* **65**(10), 3028–3038 (2016)
- [20] Lawlor, N., George, J., Bolisetty, M., Kursawe, R., Sun, L., Sivakamasundari, V., Kycia, I., Robson, P., Stitzel, M.L.: Single-cell transcriptomes identify human islet cell signatures and reveal cell-type-specific expression changes in type 2 diabetes. *Genome research* **27**(2), 208–222 (2017)
- [21] Usoskin, D., Furlan, A., Islam, S., Abdo, H., Lönnerberg, P., Lou, D., Hjerling-Leffler, J., Haeggström, J., Kharchenko, O., Kharchenko, P.V., *et al.*: Unbiased classification of sensory neuron types by large-scale single-cell rna sequencing. *Nature neuroscience* **18**(1), 145–153 (2015)
- [22] Kolodziejczyk, A.A., Kim, J.K., Tsang, J.C., Ilicic, T., Henriksson, J., Natarajan, K.N., Tuck, A.C., Gao, X., Bühler, M., Liu, P., *et al.*: Single cell rna-sequencing of pluripotent states unlocks modular transcriptional variation. *Cell stem cell* **17**(4), 471–485 (2015)
- [23] Puram, S.V., Tirosh, I., Parikh, A.S., Patel, A.P., Yizhak, K., Gillespie, S., Rodman, C., Luo, C.L., Mroz, E.A., Emerick, K.S., *et al.*: Single-cell transcriptomic analysis of primary and metastatic tumor ecosystems in head and neck cancer. *Cell* **171**(7), 1611–1624 (2017)
- [24] Muraro, M.J., Dharmadhikari, G., Grün, D., Groen, N., Dielen, T., Jansen, E., Van Gurp, L., Engelse, M.A., Carlotti, F., De Koning, E.J., *et al.*: A single-cell transcriptome atlas of the human pancreas. *Cell systems* **3**(4), 385–394 (2016)
- [25] Segerstolpe, Å., Palasantza, A., Eliasson, P., Andersson, E.-M., Andréasson, A.-C., Sun, X., Picelli, S., Sabirsh, A., Clausen, M., Bjursell, M.K., *et al.*: Single-cell transcriptome profiling of human pancreatic islets in health and type 2 diabetes. *Cell metabolism* **24**(4), 593–607 (2016)
- [26] Klein, A.M., Mazutis, L., Akartuna, I., Tallapragada, N., Veres, A., Li, V., Peshkin, L., Weitz, D.A., Kirschner, M.W.: Droplet barcoding for single-cell transcriptomics applied to embryonic stem cells. *Cell* **161**(5), 1187–1201 (2015)
- [27] Zeisel, A., Muñoz-Manchado, A.B., Codeluppi, S., Lönnerberg, P., La Manno, G.,

- Juréus, A., Marques, S., Munguba, H., He, L., Betsholtz, C., *et al.*: Cell types in the mouse cortex and hippocampus revealed by single-cell rna-seq. *Science* **347**(6226), 1138–1142 (2015)
- [28] Adam, M., Potter, A.S., Potter, S.S.: Psychrophilic proteases dramatically reduce single-cell rna-seq artifacts: a molecular atlas of kidney development. *Development* **144**(19), 3625–3632 (2017)
- [29] Schaum, N., Karkanias, J., Neff, N.F., May, A.P., Quake, S.R., Wyss-Coray, T., Darmanis, S., Batson, J., Botvinnik, O., Chen, M.B., *et al.*: Single-cell transcriptomics of 20 mouse organs creates a tabula muris: The tabula muris consortium. *Nature* **562**(7727), 367 (2018)
- [30] Single Cell Portal. <https://singlecell.broadinstitute.org/single-cell/study/SCP345/>.
- [31] Bach, K., Pensa, S., Grzelak, M., Hadfield, J., Adams, D.J., Marioni, J.C., Khaled, W.T.: Differentiation dynamics of mammary epithelial cells revealed by single-cell rna sequencing. *Nature Communications* **8**(1), 1–11 (2017)
- [32] Hrvatin, S., Hochbaum, D.R., Nagy, M.A., Cicconet, M., Robertson, K., Cheadle, L., Zilionis, R., Ratner, A., Borges-Monroy, R., Klein, A.M., *et al.*: Single-cell analysis of experience-dependent transcriptomic states in the mouse visual cortex. *Nature Neuroscience* **21**(1), 120–129 (2018)
- [33] Karagiannis, T.T., Cleary Jr, J.P., Gok, B., Henderson, A.J., Martin, N.G., Yajima, M., Nelson, E.C., Cheng, C.S.: Single cell transcriptomics reveals opioid usage evokes widespread suppression of antiviral gene program. *Nature Communications* **11**(1), 2611 (2020)
- [34] Orozco, L.D., Chen, H.-H., Cox, C., Katschke, K.J., Arceo, R., Espiritu, C., Caplazi, P., Nghiem, S.S., Chen, Y.-J., Modrusan, Z., *et al.*: Integration of eqtl and a single-cell atlas in the human eye identifies causal genes for age-related macular degeneration. *Cell reports* **30**(4), 1246–1259 (2020)